Manufacturing & Service Operations Management

Publication details, including instructions for authors and subscription information:
http://pubsonline.informs.org

Vertiport Planning for Urban Aerial Mobility: An Adaptive Discretization Approach

Kai Wang, Alexandre Jacquillat, Vikrant Vaze

To cite this article:
Kai Wang, Alexandre Jacquillat, Vikrant Vaze (2022) Vertiport Planning for Urban Aerial Mobility: An Adaptive Discretization Approach. Manufacturing & Service Operations Management 24(6):3215-3235. https://doi.org/10.1287/msom.2022.1148

https://pubsonline.informs.org/journal/msom

MANUFACTURING & SERVICE OPERATIONS MANAGEMENT
Vol. 24, No. 6, November–December 2022, pp. 3215–3235
ISSN 1523-4614 (print), ISSN 1526-5498 (online)

Vertiport Planning for Urban Aerial Mobility: An Adaptive Discretization Approach

Kai Wang,[a,*] Alexandre Jacquillat,[b] Vikrant Vaze[c]

[a] School of Vehicle and Mobility, Tsinghua University, Beijing 100084, China; [b] Sloan School of Management, Massachusetts Institute of Technology, Cambridge, Massachusetts 02142; [c] Thayer School of Engineering, Dartmouth College, Hanover, New Hampshire 03755
*Corresponding author

Contact: cwangkai@tsinghua.edu.cn, https://orcid.org/0000-0002-3040-0422 (KW); alexjacq@mit.edu, https://orcid.org/0000-0002-2352-7839 (AJ); vikrant.s.vaze@dartmouth.edu, https://orcid.org/0000-0002-8142-2461 (VV)

Received: February 8, 2021
Revised: April 8, 2022; August 2, 2022
Accepted: August 5, 2022
Published Online in Articles in Advance: September 21, 2022

https://doi.org/10.1287/msom.2022.1148

Abstract. ***Problem definition*:** Electric vertical-takeoff-and-landing (eVTOL) vehicles enable *urban aerial mobility* (UAM). This paper optimizes the number, locations, and capacities of vertiports in UAM systems while capturing interdependencies between strategic vertiport deployment, tactical operations, and passenger demand. ***Academic/practical relevance*:** The model includes a "tractable part" (based on mixed-integer second-order conic optimization) and also a nonconvex demand function. ***Methodology*:** We develop an exact algorithm that approximates nonconvex functions with piecewise constant segments, iterating between a conservative model (which yields a feasible solution) and a relaxed model (which yields a solution guarantee). We propose an *adaptive discretization* scheme that converges to a global optimum—because of the relaxed model. ***Results*:** Our algorithm converges to a 1% optimality gap, dominating static discretization benchmarks in terms of solution quality, runtimes, and solution guarantee. ***Managerial implications*:** We find that the most attractive structure for UAM is one that uses a few high-capacity vertiports, consolidating operations primarily to serve long-distance trips. Moreover, UAM profitability is highly sensitive to network planning optimization and to customer expectations, perhaps even more so than to vehicle specifications. Therefore, the success of UAM operations requires not only mature eVTOL technologies but also tailored analytics-based capabilities to optimize strategic planning and market-based efforts to drive customer demand.

Supplemental Material: The online appendix is available at https://doi.org/10.1287/msom.2022.1148.

Keywords: urban aerial mobility • network planning • adaptive discretization

1. Introduction

Major metropolitan areas face critical challenges to accommodate growing travel demand with limited infrastructure. As urban population, mobility needs and e-commerce deliveries grow rapidly, so do congestion and greenhouse gas emissions. On the positive side, urban transportation is being rapidly transformed by on-demand businesses (e.g., car-sharing, ride-sharing) and new vehicle technologies (e.g., electric, connected, autonomous vehicles). Yet, long-term sustainable transportation may require even more transformative technologies, businesses, and policies.

New opportunities are opening due to a prominent science fiction topic becoming reality: the rise of electric vertical-takeoff-and-landing (eVTOL) vehicles (Figure 1). As of early 2022, nearly 500 eVTOL designs have been proposed, with several manufacturers working toward regulatory certification (Vertical Flight Society 2021). Despite widely different designs, a few commonalities are apparent: eVTOL vehicles take off and land on limited infrastructure; they have a small payload that can accommodate a few passengers; they fly short-range operations at lower costs than helicopters, and they are electrically powered by batteries. Thus, eVTOL technologies can provide efficient small- to midrange transportation with limited greenhouse gas emissions.

The development of eVTOL vehicles gives rise to *urban aerial mobility* (UAM), with a multibillion dollar market potential (Booz Allen Hamilton 2018, Baur and Hader 2020). Cities and operators are already investing heavily into UAM. For instance, Dubai launched testing programs with eVTOL manufacturers; thousands of test flights were performed in New Zealand; Singapore deployed a UAM traffic management system; NASA partnered with several companies to accelerate UAM readiness; and several airlines ordered hundreds of eVTOL aircraft to provide airport shuttles and regional flights. A key characteristic of UAM, as opposed to ride-sharing, is the reliance on a dedicated infrastructure of *vertiports* for vehicles to take off and land (located, for instance, on building roofs or parking lots), thus creating an additional strategic challenge for future UAM operators. Whereas much attention has been devoted to vertiport design (Johnston et al. 2020), research is sparser

Figure 1. (Color online) Sample eVTOL Prototypes

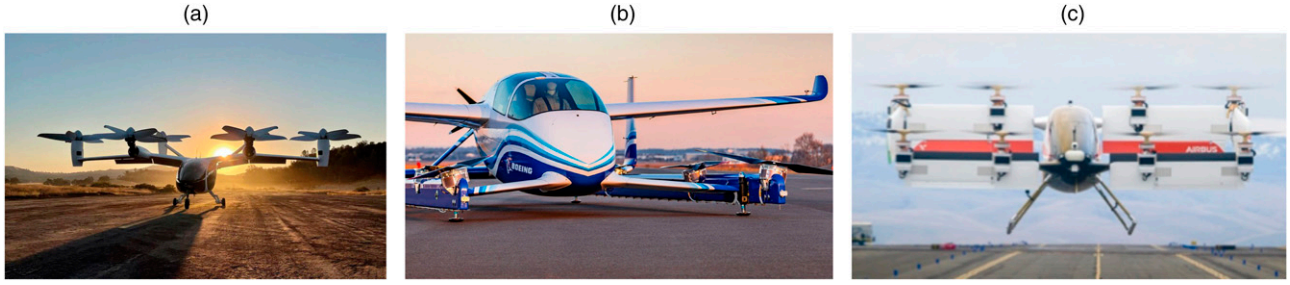

Notes. (a) Joby Aviation (2021). (b) AVweb (2019). (c) A3 by Airbus (2018).

when it comes to building vertiport networks to serve broader mobility needs.

We address this question by proposing an optimization approach to guide long-term vertiport planning in UAM networks. This problem is complicated by two critical aspects. One is the interdependencies between strategic vertiport planning and tactical operations, spanning vehicle routing, repositioning of empty vehicles, battery charging, and passenger pooling (see Section 3 for details). Another one is the interdependencies between UAM operations and passenger demand—all else equal, faster UAM trips induce higher demand. In response, this paper develops an integrated framework that captures interactions between strategic vertiport planning, tactical UAM operations, and passenger demand. From a practical standpoint, this paper addresses three main questions. First, what is the best structure of vertiport networks; in particular, should they follow a "dispersion strategy" (i.e., many scattered small-capacity vertiports to cover demand hotspots) or a "concentration strategy" (i.e., a few central high-capacity vertiports to facilitate centralized operations)? Second, what is the benefit of network optimization, as compared with easily-implementable baselines? Third, what are the key drivers of profitability for future UAM operators?

Our first contribution is formulating an integrated model of UAM vertiport planning, combining a facility location structure, a queuing network, and a demand function (Section 4). The facility location structure optimizes the number, sizes, and locations of vertiports in a metropolitan area. The queuing network replicates, albeit approximately, the tactical UAM dynamics. It augments the car-sharing model from He et al. (2017) to capture such UAM characteristics as vertiport capacities, centralized operations, endogenous battery charging, and passenger pooling. Together, these two components include linear and second-order conic constraints, which can be handled with modern solvers. In contrast, the demand function, which links supply-side operations to passenger demand, results in general constraints of the form $\boldsymbol{\alpha} \leq f(\tilde{\boldsymbol{\tau}})$, where $\tilde{\boldsymbol{\tau}}$ denotes the level of service and $\boldsymbol{\alpha}$ denotes the UAM traffic share. We propose two demand functions: one from a distributionally robust optimization model, which can be used in systems like UAM that are still in early stages of data collection, and another from a multinomial logit model, which can provide a more fine-grained characterization of passenger choice once disaggregate data become available. Either way, the function $f(\cdot)$ is nonconvex, resulting in a mixed-integer nonconvex optimization problem.

Our second contribution is an adaptive discretization algorithm to solve models combining a "tractable part" (here, a mixed-integer second-order conic program) and general constraints $\boldsymbol{\alpha} \leq f(\tilde{\boldsymbol{\tau}})$ (Section 5). The algorithm relies on a *conservative model* that provides a feasible solution, and a *relaxed model* that provides a solution guarantee. Both approximate the function $f(\cdot)$ by piecewise constant segments, resulting in the same complexity as the "tractable part". The adaptive discretization scheme enlarges the feasible region of the conservative model (to improve incumbent solutions) and reduces that of the relaxed model (to avoid local optima). Our main result shows that the adaptive discretization approach converges to a global optimum—thanks to the relaxed model. We propose an algorithm that accelerates convergence (i) by iterating between the relaxed and conservative models (to orient the search toward "promising" solutions), and (ii) by tightening piecewise constant approximations by piecewise linear approximations exploiting local convexity. The algorithm iteratively updates an upper and a lower bound until convergence, providing an exact solution approach to a broad class of mixed-integer nonconvex programs.

Our third contribution is demonstrating that the algorithm provides high-quality solutions for real-world UAM networks (Section 6). Specifically, the algorithm converges to a 1% optimality gap in 15–30 iterations. Convergence is faster when the algorithm alternates between the relaxed model and the conservative model, highlighting their synergistic roles in handling nonconvexities. Moreover, our algorithm outperforms static discretization benchmarks: it returns much better solutions than coarse discretization, and yields a Pareto improvement over granular discretization—better solutions,

faster runtimes, and tighter bounds. These performance improvements are robust across various network structures and across both demand model specifications.

Our fourth contribution is generating practical insights on UAM systems, using taxi data in New York City and census data in 12 U.S. metropolitan areas (Section 7). Our results highlight complex, and at times counterintuitive, interplay between vehicle routing, vertiport capacities, battery charging, and passenger pooling. Our findings uncover widely different UAM networks across cities, driven by geographic, urban, and commuting patterns. One commonality is that UAM primarily supports long-distance trips, serving as a more natural alternative to self-driving, airport shuttles and commuter rail rather than taxi and ride-sharing. In response to our first main practical question, UAM networks follow a "concentration strategy" around a few central vertiports to create consolidation synergies for vehicle routing and passenger pooling, at the expense of longer ingress and egress times for passengers. In particular, UAM systems do not necessarily benefit from extra vertiports—in contrast with traditional facility location. To answer our second question, optimization can improve UAM profitability by 20%–50% compared with demographics-based benchmarks. In response to our third question, UAM profitability is sensitive to vehicle specifications (e.g., costs and battery performance) but even more so to customer expectations—namely, by how much UAM needs to cut travel times to attract passengers. Ultimately, the viability of UAM operations requires not only advances in eVTOL technologies, but also tailored analytics-based capabilities to optimize strategic planning and market-based efforts to drive customer demand.

2. Literature Review

Developments in eVTOL technologies have generated several research threads (Garrow et al. 2021). The first one focuses on the design of eVTOL vehicles, trading off range, endurance, thrust, power, noise, and economic performance (Brown and Harris 2018, Ha et al. 2019). A second thread deals with operations at the vertiports by optimizing the trajectories of eVTOL aircraft (Kleinbekman et al. 2018, Pradeep and Wei 2018) and estimating vertiport capacities (Vascik and Hansman 2019). A third thread uses surveys to estimate customers' willingness to pay (Binder et al. 2018) and characterize mode choices between self-driving, autonomous cars and UAM (Garrow et al. 2019). A last thread characterizes broader needs of UAM in terms of certification, infrastructure, traffic management, and operating rules (Uber Elevate 2016, Vascik and Hansman 2017).

This paper departs from this body of work by tackling the vertiport planning problem. A seemingly analogous problem is airline network design (Jaillet et al. 1996, Lederer and Nambimadom 1998), but vertiport planning is different due to the point-to-point (versus hub-and-spoke) and on-demand (versus scheduled) UAM operations. Vertiport planning also relates to the design of on-demand bike-sharing systems (Kabra et al. 2020) and car-sharing systems (Boyaci et al. 2015). In UAM, a few papers have studied vertiport network planning by clustering commuting data using k-means or p-median algorithms (Lim and Hwang 2019, Willey and Salmon 2021). In contrast, we optimize vertiport networks by means of an integrated model that captures downstream UAM operations and UAM demand as opposed to solely relying on demographic data. As our results show, this approach yields significant benefits over demographic-based benchmarks.

Related to our paper, He et al. (2017) optimize region design in electric car-sharing. We leverage two main ideas from this paper. First, we use a queuing network (see also Adelman 2007, Pavone 2015) to model vehicle operations given the vertiport network. Second, we use a demand function with a distributionally robust optimization formulation to capture uncertainty regarding future utilization—which is particularly relevant in a brand new system like UAM. Yet, our paper departs in four major ways, to capture: (i) centralized vehicle dispatch, as opposed to user-driven operations; (ii) capacitated vertiports, as opposed to free-floating operations; (iii) endogenous battery charging dynamics as a function of vehicle utilization; and (iv) demand-supply interdependencies. This last point leads to our nonconvex demand function that motivates our solution algorithm.

Methodologically, our adaptive discretization approach relates to time discretization in logistics. Specifically, Boland et al. (2017) propose a method to address continuous-time network optimization problems by solving a relaxed variant problem on partially time-expanded networks and by iteratively refining time discretization until convergence (Lagos et al. 2020, Vu et al. 2020). They propose a mixed-integer program to identify which time points to add, and to check whether each incumbent solution is optimal. Similarly, our paper develops an exact algorithm that yields a provably global optimal solution by dynamically adjusting the granularity of discretization. However, it also exhibits three differences from Boland et al. (2017). First, we tackle mixed-integer nonconvex programs, as opposed to large-scale mixed-integer linear programs. Second, our conservative model yields a feasible solution at each iteration, as opposed to reconstructing one from the relaxed solution. Third, our algorithm adjusts the discretization by leveraging the solutions of the conservative model (to exploit good solutions) and the relaxed model (to avoid local optima).

3. Background and Assumptions

This section outlines the main components of UAM systems. Obviously, many uncertainties remain, depending

on the exact business models that will prevail. Nevertheless, a few operating characteristics are emerging from industry reports and UAM operators' press releases.

On the vehicle side, eVTOL aircraft leverage advances in electric propulsion to power vertical-takeoff-and-landing flights. Existing prototypes rely on various designs (e.g., fixed wings with pivoting motors, tilt-wing configurations, wingless multicopters), with various payloads (2–20 seats, typically 4–6), speeds (50–200 miles per hour) and ranges (20–250 miles). Across these designs, operating costs are projected to be highly competitive (estimated at \$2.50-4.50 per seat-mile in the near term and \$0.50-2.50 in the long term versus \$6-8 for helicopters).

On the infrastructure side, vertiports comprise a takeoff and landing area (where flights originate and terminate), a parking area (where eVTOL aircraft are cleaned, receive maintenance, and charge their batteries), and a terminal area (where passengers wait for their trip). Current prototypes vary significantly: small designs have one takeoff and landing area and a few parking spaces, whereas large ones comprise up to ten takeoff and landing areas and 20 parking spaces.

On the operations side, most UAM operators are aspiring to become vertically integrated system providers. For instance, Joby Aviation, an eVTOL manufacturer, acquired Uber Elevate and partnered with REEF (a parking operator) and the Neighborhood Property Group (a real estate company). Integrated UAM operators can thus control vertiport, vehicle, and passenger operations centrally. First, they can assign each passenger to departure and arrival vertiports ("passenger-vertiport matching"). Second, they pool passengers together to take advantage of multiseat eVTOL aircraft ("passenger pooling"). Third, they can manage eVTOL fleets by coordinating vehicle dispatches, repositioning trips, and battery charging.

From the passengers' standpoint, a UAM trip evolves in four steps: (i) ground travel from the origin to a departure vertiport, (ii) passenger pooling, (iii) flight between departure and arrival vertiports, and (iv) ground travel from the arrival vertiport to the destination. Therefore, UAM attractiveness depends not only on actual flying times but also on ground travel times and pooling times. Moreover, to serve passengers, the UAM operator must have an eVTOL aircraft available at the departure vertiport; otherwise, passengers can wait longer or use a different means of transportation, resulting in service deterioration that we refer to as "detour times."

These dynamics separate UAM from existing transportation systems. Unlike airlines, UAM involves on-demand operations with small vehicles as opposed to scheduled large-capacity flights. Unlike car-sharing, UAM relies on centralized fleet management and passenger pooling, as opposed to customer-driven operations. Unlike ride-sharing, UAM relies on a dedicated infrastructure of vertiports, as opposed to free-floating operations.

This paper thus proposes a new model to optimize UAM vertiport planning. Given the strategic nature of the problem, our model solves for the "end-state" network, as opposed to dynamic network expansions (which would require a multistage stochastic optimization, hindering tractability). Moreover, given the problem's complexity and the lack of real-world data, our model relies on a queuing network to capture first-order operational dynamics, based on the following assumptions:

- We model passenger demand via a Poisson process on each origin-destination pair.
- The UAM operator assigns each passenger to a departure vertiport and an arrival vertiport and arranges ground transportation to the departure vertiport and from the arrival vertiport. Ground travel times are exogeneous to UAM operations.
- We model passenger pooling via a probabilistic split: upon each passenger's arrival, the UAM operator arranges a service (to all passengers currently waiting on the same vertiport pair) with a given probability. This is motivated by the variable number of demand realizations leading to a passenger pool (e.g., a single passenger versus a family; the UAM operator operating full versus partial flights). Our random splitting process captures such variability while retaining tractability—by propagating Poisson dynamics from passenger demand to flight demand.
- We characterize flight repositioning as a Poisson process with an endogenous arrival rate on each vertiport pair. This assumption also maintains Poisson dynamics at the flight level.
- We ensure that, at each vertiport, the total charging time is sufficient to power all departing flights. The model thus does not keep track of each vehicle's state of charge (consistent with the flow-based queuing network) but still captures the endogeneity of battery charging.
- Customers are infinitely impatient: passengers are lost if no aircraft is available upon completion of the pooling process. In that case, the UAM operator arranges a trip to the destination via ground transportation. This assumption is consistent with the literature (Adelman 2007, Pavone 2015, He et al. 2017) and necessary to maintain one-sided queuing dynamics.
- We consider an uncapacitated queue at each vertiport and cap the probability of the vertiport operating beyond its capacity to a small threshold (5%). Practically, this assumption is justified by the fact that vehicles can wait in the airspace or be repositioned to nearby vertiports. Technically, it avoids complex nonlinear expressions from capacitated queuing models.
- We consider linear passenger utility, trading off fares, and worst-case expected trip times over all possible options of vertiport pairs for a given origin-destination pair. Trip times capture ground and in-flight travel, pooling, and detour times (when no aircraft is available).

Table 1. Main Characteristics of UAM Systems and Our Modeling Framework

Item	Physical component	Modeling feature	Novel?
Network planning	Fixed infrastructure	Vertiport deployment and capacity variables	Yes
	Vehicle fleet	eVTOL fleet sizing variables	No
UAM operations	Network-wide interdependencies	Queuing network	No
	Empty vehicle repositioning	Repositioning demand	No
	Coordinated ground and air transport	Passenger-vertiport matching	Yes
	Battery charging at vertiports	Endogenous charging based on utilization	Yes
	Vehicle sharing	Passenger pooling at departure vertiports	Yes
Customer demand	Uncertain demand	Distributionally robust optimization	No
	Supply-dependent demand	Endogenous demand function $\boldsymbol{\alpha} \leq f(\tilde{\boldsymbol{\tau}})$	Yes

• The eVTOL technologies and UAM fares are exogenous to the model.

Although simplifying, these assumptions capture the endogeneity of UAM operations and passenger demand in network planning optimization. Moreover, they lie in the tactical dynamics of UAM systems ("wait-and-see" decisions that will be implemented later on), as opposed to the strategic decisions surrounding vertiport planning ("here-and-now" decisions that need to be implemented in the shorter term). They can then be relaxed to optimize UAM operations at the tactical level, by fixing vertiport networks and optimizing routing, pricing, pooling, and so on.

Table 1 summarizes the key components and novelties of our modeling framework. The most significant one is the integration of an endogenous demand function into vertiport network optimization—leading to our mixed-integer nonconvex optimization model and our algorithm.

4. UAM Vertiport Planning Model

The model's primary decisions capture the number, locations, and capacities of vertiports; auxiliary decisions reflect the fleet size, UAM operations, and customer demand (Figure 2).

As described in Section 3, UAM operations involve the following: (i) passenger-vertiport matching, translating origin-destination (O-D) demand into vertiport-pair demand; (ii) passenger pooling, translating vertiport-pair demand into flight demand; and (iii) fleet management (i.e., vehicle routing, repositioning, and charging). We define *service reliability* as the probability that an aircraft is available when a flight is required (otherwise, passengers travel by ground transportation). These three steps define the three components of O-D trip time: travel time, wait time, and detour time.

4.1. Strategic Vertiport Deployment and Fleet Sizing

Let $\mathcal{N}$ denote a set of candidate vertiport locations. The capacity of a vertiport corresponds to the number of eVTOL aircraft that can be parked and charged. For each $i \in \mathcal{N}$, we consider several possible capacity values, indexed by $h \in \mathcal{H}_i$ and denoted by Q_{ih}. We define the following variables:

$z_{ih} = 1$ if a vertiport is built in location $i \in \mathcal{N}$ with capacity Q_{ih}, for $h \in \mathcal{H}_i$; 0 otherwise.

Γ = number of vehicles operating across the full network.

Equation (1) ensures that no more than one capacity level is selected at each vertiport. Equation (2) states that the network has sufficient capacity to accommodate the entire fleet:

$$\sum_{h \in \mathcal{H}_i} z_{ih} \leq 1, \quad \forall i \in \mathcal{N}, \tag{1}$$

$$\sum_{i \in \mathcal{N}} \sum_{h \in \mathcal{H}_i} Q_{ih} z_{ih} \geq \Gamma. \tag{2}$$

4.2. Customer Demand and Passenger Flows

We partition a metropolitan area into a set $\mathcal{R}$ of small regions. Customer demand realizes between an origin $o \in \mathcal{R}$ and a destination $d \in \mathcal{R}$. We define passenger-vertiport matching variables:

$y_{o,i,j,d} = 1$ if flights from $i \in \mathcal{N}$ to $j \in \mathcal{N}$ serve demand from $o \in \mathcal{R}$ to $d \in \mathcal{R}$; 0 otherwise.

Equations (3) and (4) ensure that matching variables can be active only for built vertiports:

$$y_{o,i,j,d} \leq \sum_{h \in \mathcal{H}_i} z_{ih}, \quad \forall o, d \in \mathcal{R}, \ \forall i, j \in \mathcal{N}, \tag{3}$$

$$y_{o,i,j,d} \leq \sum_{h \in \mathcal{H}_j} z_{jh}, \quad \forall o, d \in \mathcal{R}, \ \forall i, j \in \mathcal{N}. \tag{4}$$

Each (o, d) pair can be "split" into several vertiport pairs. The worst-case expected trip time, denoted by τ_{od} on O-D pair (o, d), is given as follows, where M is a large positive number:

$$\tau_{od} \geq \left(t^g_{oi} + t^f_{ij} + t^g_{jd}\right) + \delta_{ij} + \nu_{i,j,d} + (y_{o,i,j,d} - 1)M, \quad \forall o, d \in \mathcal{R}, \ \forall i, j \in \mathcal{N}. \tag{5}$$

The first term reflects the (exogenous) travel time summing ground travel times from o to i (t^g_{oi}) and from j to d

Figure 2. Modeling Architecture

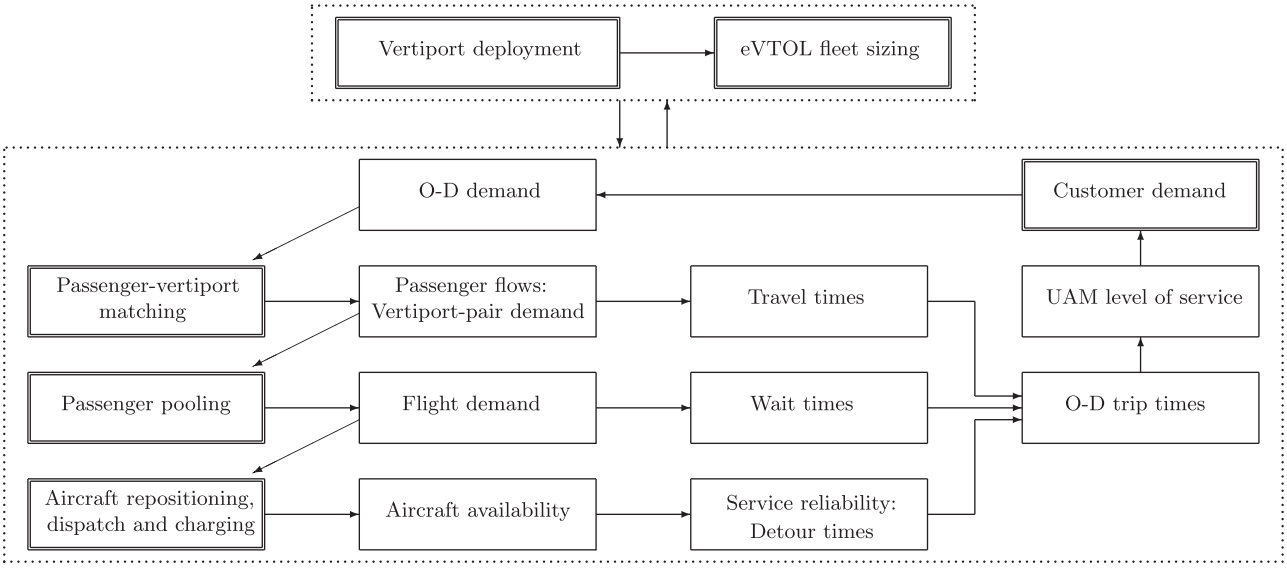

Note. Decision variables are indicated in doubled squares.

(t^g_{jd}), and the flying time from i to j (t^f_{ij}). The second term, δ_{ij}, denotes the (endogenous) expected pooling time at vertiport i for passengers traveling to vertiport j. The third term, $v_{i,j,d}$, refers to the (endogenous) expected detour time if no vehicle is available at vertiport i. The last term enforces the constraint if $y_{o,i,j,d} = 1$, and ensures that it is satisfied otherwise.

Let $\alpha_{od} \in [0,1]$ denote the UAM traffic share, that is, the fraction of passengers on O-D pair (o, d) traveling with UAM. We define a constraint $\boldsymbol{\alpha} \leq f(\tilde{\boldsymbol{\tau}})$, where $\tilde{\tau}_{od}$ denotes the level of service on O-D pair (o, d) (decreasing with the trip time τ_{od}). We consider two demand functions $f(\cdot)$, based on a distributionally robust optimization model and a multinomial logit model (Section 4.4).

4.3. Model of UAM Operations

4.3.1. Queuing Network. To estimate operating profits from the vertiport network (described by $\boldsymbol{z}$) and customer demand (described by $\boldsymbol{\alpha}$), we use a queuing network with vehicles as commodities, inspired by Adelman (2007), Pavone (2015), and He et al. (2017). Figure 3 shows the closed queuing network and an open network approximation that relates UAM operations to fleet size.

We create three sets of vehicle queues. Each node $i \in \mathcal{N}$ hosts a *vertiport queue*. When a vehicle departs to transport passengers from vertiport i toward vertiport j, it enters a *transit queue* $I(i, j)$, modeled as an uncapacitated $\cdot/G/\infty$ system (where G is a flying time distribution). To mitigate spatial imbalances, we create a *repositioning*

Figure 3. Closed and Open Queuing Networks, with Vertiport, Transit, and Repositioning Queues

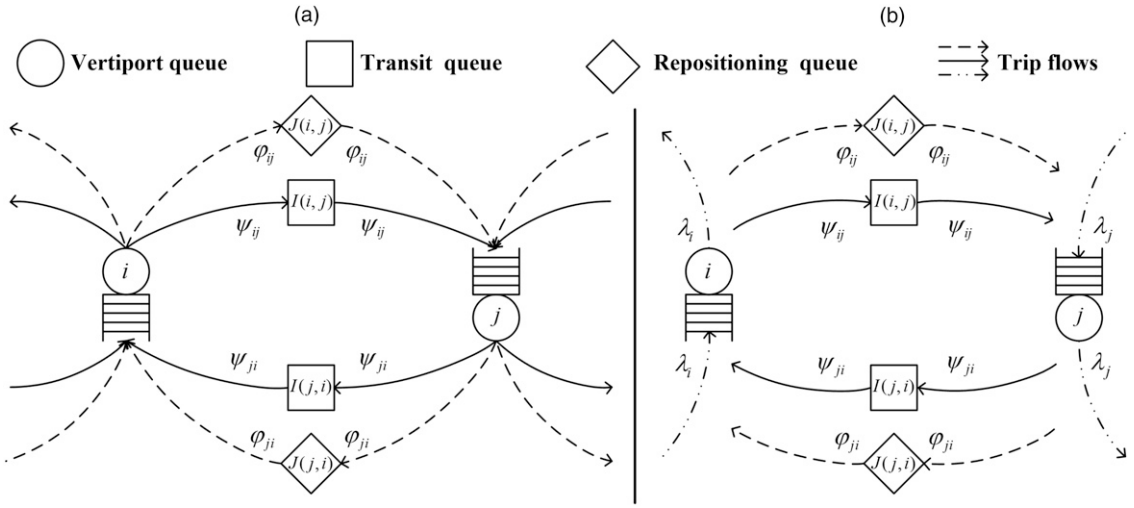

queue $J(i, j)$, also an uncapacitated $\cdot/G/\infty$ system. Any vehicle leaving transit queue $I(i, j)$ or repositioning queue $J(i, j)$ joins vertiport queue j. Each vertiport queue is a capacitated $\cdot/M/1$ queue, where "service" corresponds to vehicles leaving vertiport j (with or without passengers) and the "service rate" is the flight demand rate.

4.3.2. Passenger Flows. Let D_{od} be the overall passenger demand rate on O-D pair (o, d). Therefore, UAM demand realizes at rate $\alpha_{od}D_{od}$. Let $\pi_{o,i,j,d}$ be the fraction of customers on O-D pair (o, d) assigned to vertiport pair (i, j). The passenger demand rate on vertiport pair (i, j), χ_{ij}, is given by

$$\chi_{ij} = \sum_{o,d\in\mathcal{R}} D_{od}\pi_{o,i,j,d}, \quad \forall i,j \in \mathcal{N}. \tag{6}$$

Equation (7) ensures that the O-D pair (o, d) is matched to vertiport pair (i, j) if $\pi_{o,i,j,d} > 0$. Equation (8) ensures that passenger flows are sufficient to capture the UAM traffic share:

$$\pi_{o,i,j,d} \le y_{o,i,j,d}, \quad \forall o,d \in \mathcal{R}, i,j \in \mathcal{N}. \tag{7}$$

$$\sum_{i,j\in\mathcal{N}} \pi_{o,i,j,d} \ge \alpha_{od}, \quad \forall o,d \in \mathcal{R}. \tag{8}$$

4.3.3. Passenger Pooling. Upon each passenger's arrival at the departure vertiport, the operator serves all passengers traveling to the same vertiport with probability $1/n$, where n is the average number of passengers per flight. Flight demand on vertiport pair (i, j) thus follows a Poisson process, with rate χ_{ij}/n. Expected customer wait times are thus $\delta_{ij} = (1/n)\cdot 0 + (1-(1/n))\cdot(n/\chi_{ij}) = ((n-1)/\chi_{ij})$ for all $i,j \in \mathcal{N}$ such that $\chi_{ij} > 0$. To address cases with $\chi_{ij} = 0$, we define a small $\varepsilon > 0$ and $\chi^+_{ij} > 0$ as

$$\chi^+_{ij} = \chi_{ij} + \varepsilon, \quad \forall i,j \in \mathcal{N}. \tag{9}$$

Lemma 1. *The constraints* $\delta_{ij} \ge ((n-1)/\chi^+_{ij})$ *can be written as second-order cone constraints as follows*:

$$\left\| \begin{matrix} 2\sqrt{n-1} \\ \delta_{ij} - \chi^+_{ij} \end{matrix} \right\|_2 \le \delta_{ij} + \chi^+_{ij}, \quad \forall i,j \in \mathcal{N}. \tag{10}$$

4.3.4. Detour Times. We define a set of discretized service reliability levels $(\rho_s)_{s\in\mathcal{S}}$ (e.g., $\rho_1 = 0.1, \rho_2 = 0.2, \cdots, \rho_9 = 0.9$). At each constructed vertiport i, its service reliability is $\sum_{s\in\mathcal{S}}\rho_s\omega_{is}$, where

$$\omega_{is} = 1 \text{ if vertiport } i \in \mathcal{N} \text{ has the } s^{\text{th}}(s \in \mathcal{S}) \text{ level of service reliability; } 0 \text{ otherwise.}$$

Equation (11) sets one reliability level at each constructed vertiport, that is, whenever $\sum_{h\in\mathcal{H}_i} z_{ih} = 1$:

$$\sum_{s\in\mathcal{S}} \omega_{is} = \sum_{h\in\mathcal{H}_i} z_{ih}, \quad \forall i \in \mathcal{N}. \tag{11}$$

With probability $1 - \sum_{s\in\mathcal{S}}\rho_s\omega_{is}$, no aircraft is available at vertiport i when a pool of customers is ready to depart. In that case, customers traveling to destination d incur a detour time equal to the ground travel time from i to d (t^g_{id}) minus the remaining time with UAM ($t^f_{ij} + t^g_{jd}$). That is,

$$\nu_{ijd} = \left(1 - \sum_{s\in\mathcal{S}} \rho_s\omega_{is}\right)(t^g_{id} - t^f_{ij} - t^g_{jd}), \quad \forall i,j \in \mathcal{N}, d \in \mathcal{R}. \tag{12}$$

We denote by ψ_{ij} the *realized* flight flow from vertiport i to vertiport j, as $\psi_{ij} = \sum_{s\in\mathcal{S}}\rho_s\omega_{is}(\chi_{ij}/n)$. We linearize this expression as follows, where M is a large positive number:

$$\rho_s\frac{\chi_{ij}}{n} - (1-\omega_{is})M \le \psi_{ij} \le \rho_s\frac{\chi_{ij}}{n} + (1-\omega_{is})M, \quad \forall i,j \in \mathcal{N}, s \in \mathcal{S}, \tag{13}$$

$$\psi_{ij} \le \frac{\chi_{ij}}{n}, \quad \forall i,j \in \mathcal{N}. \tag{14}$$

4.3.5. Fleet Repositioning. Let φ_{ij} be the rate of repositioning trips from vertiport i to vertiport j. Then, at each vertiport i, the following equations balance the aircraft flows:

$$\sum_{j\in\mathcal{N}}(\psi_{ji} + \varphi_{ji}) = \sum_{j\in\mathcal{N}}(\psi_{ij} + \varphi_{ij}), \quad \forall i \in \mathcal{N}. \tag{15}$$

4.3.6. Vehicle Fleet. We apply the fixed-population-mean method from Whitt (1984) to approximate fleet size in an open queuing network. This follows He et al. (2017), but we design a new open-loop approximation because vehicles charge at the vertiports rather than at separate charging stations.

Our open queuing network (Figure 3(b)) disconnects vertiport queues from transit and repositioning queues. Vehicle arrivals follow a Poisson process with rate $\lambda_i = \sum_{j\in\mathcal{N}}(\psi_{ji} + \varphi_{ji})$ at each vertiport i, with rate ψ_{ij} in each transit queue $I(i, j)$, and with rate φ_{ij} in each repositioning queue $J(i, j)$. Vertiport queues thus become $M/M/1$ systems, and transit and repositioning queues become $M/G/\infty$ systems. The expected number of vehicles at vertiport $i \in \mathcal{N}$ equals $\sum_{s\in\mathcal{S}}((\rho_s)/1-\rho_s)\,\omega_{is}$ ($M/M/1$ formula). From Little's law, the average number of vehicles in each transit queue $I(i, j)$ (respectively, repositioning queue $J(i, j)$) equals $t^f_{ij}\psi_{ij}$ (respectively, $t^f_{ij}\varphi_{ij}$). The fleet size constraint becomes

$$\sum_{i\in\mathcal{N}}\sum_{s\in\mathcal{S}}\frac{\rho_s}{1-\rho_s}\omega_{is} + \sum_{i,j\in\mathcal{N}} t^f_{ij}(\psi_{ij} + \varphi_{ij}) \le \Gamma. \tag{16}$$

4.3.7. Vertiport Capacity. Consider a vertiport with capacity Q_{ih}. Because the queue at vertiport i is $M/M/1$,

the probability of exceeding the capacity is $(\sum_{s\in\mathcal{S}} \rho_s \omega_{is})^{Q_{ih}+1}$. We cap this probability to a small threshold γ (set to 5%) via the following linear constraints:

$$\sum_{s\in\mathcal{S}} \rho_s \omega_{is} \le \sum_{h\in\mathcal{H}_i} \gamma^{\frac{1}{Q_{ih}+1}} z_{ih}, \quad \forall i \in \mathcal{N}. \tag{17}$$

4.3.8. Battery Charging. We extend the approach from He et al. (2017) by endogenizing charging decisions with vehicle utilization, as opposed to treating them exogenously. Let b^{chg} and b^{dpt} be the battery charging and depletion rates. Recall that the expected number of vehicles at vertiport $i \in \mathcal{N}$ is $\sum_{s\in\mathcal{S}}((\rho_s)/1-\rho_s)\omega_{is}$. From Little's law, the average time spent at vertiport i is thus $\sum_{s\in\mathcal{S}}((\rho_s)/1-\rho_s)(\omega_{is}/\lambda_i)$. Similarly, because the expected number of vehicles traveling between vertiports i and j is $t^f_{ij}(\psi_{ij}+\varphi_{ij})$, the average flying time after leaving vertiport i is $(\sum_{j\in\mathcal{N}} t^f_{ij}(\psi_{ij}+\varphi_{ij})/\sum_{j\in\mathcal{N}}(\psi_{ij}+\varphi_{ij}))$. However, from Equation (15), $\sum_{j\in\mathcal{N}}(\psi_{ij}+\varphi_{ij}) = \sum_{j\in\mathcal{N}}(\psi_{ji}+\varphi_{ji}) = \lambda_i$. After multiplication by λ_i, we get

$$\sum_{s\in\mathcal{S}} \frac{\rho_s}{1-\rho_s}\omega_{is} \ge \frac{b^{\text{dpt}}}{b^{\text{chg}}} \sum_{j\in\mathcal{N}} t^f_{ij}(\psi_{ij}+\varphi_{ij}), \quad \forall i \in \mathcal{N}. \tag{18}$$

4.4. Customer Demand

Let p_{od} and q_{od} denote the (exogenous) fares of UAM and the best ground option on O-D pair (o, d). We define the following utility functions, where U_{od} (respectively, $\overline{U}_{od}$) is the utility of a customer when using UAM (respectively, ground transportation) on O-D pair (o, d), $V_{od} > 0$ is the value of a trip, $b > 0$ is the time sensitivity of customers, and t^g_{od} is the trip time from o to d using ground transportation:

$$U_{od} = V_{od} - p_{od} - b \cdot \tau_{od}, \quad \forall o, d \in \mathcal{R}, \tag{19}$$

$$\overline{U}_{od} = V_{od} - q_{od} - b \cdot t^g_{od}, \quad \forall o, d \in \mathcal{R}. \tag{20}$$

The utility function could easily capture other (exogenous) amenities, but in the absence of further information, we restrict our attention to the core tradeoff between prices and expected trip times.

4.4.1. Multinomial Logit Model. Under multinomial logit model (MNL), each passenger traveling on O-D pair (o, d) will choose the UAM service with probability $((e^{U_{od}})/e^{U_{od}} + e^{\overline{U}_{od}})$. The demand function is thus given by

$$\alpha_{od} \le \frac{e^{-p_{od}+b\cdot\tilde{\tau}_{od}}}{e^{-p_{od}+b\cdot\tilde{\tau}_{od}} + e^{-q_{od}-b\cdot t^g_{od}}}, \quad \forall o, d \in \mathcal{R},$$
$$\text{where } \tilde{\tau}_{\text{od}} = -\tau_{\text{od}}. \tag{21}$$

4.4.2. Distributionally Robust Optimization (DRO). Customers choose the UAM service if $U_{od} \ge \overline{U}_{od}$, that is, if $\tau_{od} \le (1-\theta_{od})t^g_{od}$, where $\theta_{od} = ((p_{od}-q_{od})/b \cdot t^g_{od})$ characterizes the relative travel time reduction needed for UAM to attract customers. For the UAM operator, θ_{od} can be viewed as a random variable (on each O-D pair). The traffic share is given by a chance constraint:

$$\alpha_{od} \le \mathbb{P}\left(\theta_{od} \le 1 - \frac{\tau_{od}}{t^g_{od}}\right), \quad \forall o, d \in \mathcal{R}. \tag{22}$$

If the distribution $\mathbb{P}$ was known, Equation (22) would be the customer demand function. Instead, we adopt a moment-based DRO approach. Let μ_{od} and $(\sigma_{od})^2$ be the mean and variance of θ_{od}, which can be estimated from ongoing customer surveys (Binder et al. 2018, Garrow et al. 2019). Let $\mathcal{P}(\mu_{od}, \sigma_{od})$ be the corresponding set of distributions. We replace Equation (22) by

$$\alpha_{od} \le \inf_{F\in\mathcal{P}(\mu_{od},\sigma_{od})} F\left(1 - \frac{\tau_{od}}{t^g_{od}}\right), \quad \forall o, d \in \mathcal{R}. \tag{23}$$

Proposition 1 linearizes Equation (23) based on the result from El Ghaoui et al. (2003). It also leverages the passenger flow constraints (Equations (7) and (8)) to tighten the formulation by eliminating auxiliary variables and big-M parameters. In addition, Equation (24) enables model simplifications by fixing variables and eliminating constraints. Details are provided in Online Appendix EC.1.2.

Proposition 1. *Equation (23) is equivalent to*

$$\alpha_{od} \le \frac{(\tilde{\tau}_{od})^2}{1+(\tilde{\tau}_{od})^2}, \quad \forall o, d \in \mathcal{R},$$
$$\text{where } \tilde{\tau}_{od} = \frac{1}{\sigma_{od}}\left(1 - \frac{\tau_{od}}{t^g_{od}} - \mu_{od}\right). \tag{24}$$

4.4.3. Summary. The two demand functions capture supply-demand interdependencies via MNL (Equation (21)) and DRO (Equation (24)). Both can be represented by the following function:

$$\alpha_{od} \le f(\tilde{\tau}_{od}) \text{ or } \tilde{\tau}_{od} \ge f^{-1}(\alpha_{od}),$$
$$\text{where } \tilde{\tau}_{od} = -\tau_{od} \text{ (MNL) or } \tilde{\tau}_{od} = \frac{1 - \frac{\tau_{od}}{t^g_{od}} - \mu_{od}}{\sigma_{od}} \text{ (DRO).} \tag{25}$$

Although the MNL and DRO functions rely on different modeling frameworks, they are both increasing—so passenger demand increases with level of service—and they both exhibit an S-curve relationship between level of service and demand. We will exploit these properties in Section 5.

Lemma 2. *Let f be the demand function derived from MNL or DRO (Equation (25)).*

• *Monotonicity: $f(\cdot)$ is invertible, and $f^{-1}(\cdot)$ is increasing over $(0,1)$.*
• *S-curve: There exists $\zeta \in (0,1)$ such that $f^{-1}(\cdot)$ is concave over $[0,\zeta]$ and convex over $[\zeta,1]$.*

4.5. Full Formulation

The profit-maximization objective is given as follows, where g_{ih}, c^E, and c^F_{ij} denote unit vertiport, vehicle, and flight costs, respectively (in daily units), and $r_i \in \mathcal{R}$ is the region of vertiport $i \in \mathcal{N}$:

$$\Pi = \underbrace{\sum_{o,d\in\mathcal{R}} p_{od} D_{od} \alpha_{od}}_{\text{revenue}} - \underbrace{\sum_{i\in\mathcal{N}} \sum_{h\in\mathcal{H}_i} g_{ih} z_{ih}}_{\text{vertiport cost}} - \underbrace{c^E \Gamma}_{\text{fleet cost}} - \underbrace{\sum_{i,j\in\mathcal{N}} c^F_{ij}(\psi_{ij}+\varphi_{ij})}_{\text{flight cost}}$$
$$- \underbrace{\sum_{o,d\in\mathcal{R}} \sum_{i,j\in\mathcal{N}} D_{od}(q_{o,r_i} + q_{r_j,d})\pi_{o,i,j,d}}_{\text{ground transport cost}}$$
$$- \underbrace{\sum_{o,d\in\mathcal{R}} \sum_{i,j\in\mathcal{N}} D_{od}(q_{r_i,d} - q_{r_j,d} + c^P_{id})\xi_{o,i,j,d}}_{\text{cost of unsatisfied demand}}. \quad (26)$$

For the last term—the cost for unsatisfied demand—recall that a fraction $(1 - \sum_{s\in\mathcal{S}} \rho_s \omega_{is})$ of demand is lost at vertiport $i \in \mathcal{N}$ due to aircraft unavailability. In this case, the firm bears a ground transport cost from vertiport i to destination d, as well as a penalty for customer dissatisfaction c^P_{id}. To capture this, we denote by $\xi_{o,i,j,d} = \pi_{o,i,j,d}(1 - \sum_{s\in\mathcal{S}} \rho_s \omega_{is})$ the fraction of lost trips on O-D pair (o, d) between vertiports i and j. This is linearized, using a large positive number M, as follows:

$$(1-\rho_s)\pi_{o,i,j,d} - (1-\omega_{is})M \le \xi_{o,i,j,d} \le (1-\rho_s)\pi_{o,i,j,d} + (1-\omega_{is})M, \quad \forall o,d \in \mathcal{R}, i,j \in \mathcal{N}, s \in \mathcal{S}, \quad (27)$$
$$\xi_{o,i,j,d} \le \pi_{o,i,j,d}, \quad \forall o,d \in \mathcal{R}, i,j \in \mathcal{N}. \quad (28)$$

The full problem is formulated as follows. Tight big-M parameters are set in Online Appendix EC.1.3. This model is a mixed-integer nonconvex program, comprising a "tractable part" based on mixed-integer second-order conic programming (MISOCP) and the nonconvex demand constraints $\boldsymbol{\alpha} \le f(\tilde{\boldsymbol{\tau}})$:

max Π (Equation (26)),
s.t. Network construction and demand-vertiport matching constraints: Equations (1)–(4),
Customer demand constraints: Equations (5) and (24) (or (21)),
UAM operating constraints: Equations (6)–(18) and (27)–(28),
$\boldsymbol{\tau}, \tilde{\boldsymbol{\tau}}, \boldsymbol{\alpha}, \boldsymbol{\pi}, \boldsymbol{\chi}, \boldsymbol{\chi}^+, \boldsymbol{\psi}, \boldsymbol{\varphi}, \boldsymbol{\delta}, \boldsymbol{\nu}, \boldsymbol{\xi}$ non-negative; Γ integer; $\boldsymbol{y}, \boldsymbol{z}, \boldsymbol{\omega}$ binary.

5. Adaptive Discretization Algorithm

Our optimization model, referred to as $[M^*]$, admits the following form, where $\boldsymbol{c}^1, \boldsymbol{c}^2$ are nonnegative parameters, $\boldsymbol{\alpha}$ and $\tilde{\boldsymbol{\tau}}$ are as defined in Section 4, and $\boldsymbol{u}$ contains all other decision variables:

$$\max_{\boldsymbol{u},\boldsymbol{\alpha},\tilde{\boldsymbol{\tau}}} \quad (\boldsymbol{c}^1)^T \boldsymbol{\alpha} - (\boldsymbol{c}^2)^T \boldsymbol{u}, \quad (29)$$
$$\text{s.t.} \quad \boldsymbol{F}\boldsymbol{u} + \boldsymbol{G}\boldsymbol{\alpha} + \boldsymbol{H}\tilde{\boldsymbol{\tau}} = \boldsymbol{w}, \quad (30)$$
$$\|\boldsymbol{A}_{ij}\boldsymbol{u} + b_{ij}\|_2 \le \boldsymbol{e}_{ij}^T \boldsymbol{u} + d_{ij}, \quad \forall i,j \in \mathcal{N}, \quad (31)$$
$$f^{-1}(\boldsymbol{\alpha}) \le \tilde{\boldsymbol{\tau}}. \quad (32)$$

To handle the models' nonconvexities (Equation (32)), we design an exact solution algorithm based on adaptive discretization. The algorithm iterates between models of the same complexity as the tractable part (here, MISOCP). The algorithm updates a feasible solution and an optimality gap at each iteration, until convergence to an optimal solution (within a prespecified tolerance). We first describe the principles of our solution approach in a generic nonconvex optimization setting (Section 5.1), and then detail it for our UAM network planning problem (Sections 5.2–5.5).

5.1. General Principles

To outline our solution approach, let us consider a generic nonconvex optimization problem:

$$[G^*] \qquad \max\{g(\boldsymbol{x}) : \boldsymbol{x} \in \mathcal{X};\ h(\boldsymbol{x}) \ge 0\}.$$

Assuming that optimizing linear functions over $\mathcal{X}$ is practically tractable, the main complexity lies in the (nonconvex) structures of $g(\cdot)$ and $h(\cdot)$. We rely on discretization to build a "pessimistic" piecewise constant approximation, yielding a conservative model $[G_C]$, and an "optimistic" piecewise constant approximation, yielding a relaxed model $[G_R]$. Let us consider a partition $(\mathcal{I}^l)_{l=1,\cdots,L}$ of $\mathcal{X}$. We denote by $\underline{g}^l$ (respectively, $\overline{g}^l$) the infimum (respectively, supremum) of $g(\cdot)$ over $\mathcal{I}^l$, and define

$$[G_C] \qquad \max\left\{\sum_{l=1}^{L} \underline{g}^l \mathbf{1}(\boldsymbol{x} \in \mathcal{I}^l) : \boldsymbol{x} \in \bigcup_{l=1}^{L} \mathcal{J}^l_C\right\},$$
$$\text{where : } \mathcal{J}^l_C = \begin{cases} \mathcal{I}^l & \text{if } h(\boldsymbol{x}') \ge 0, \ \forall \boldsymbol{x}' \in \mathcal{I}^l \\ \emptyset & \text{otherwise} \end{cases}$$
$$[G_R] \qquad \max\left\{\sum_{l=1}^{L} \overline{g}^l \mathbf{1}(\boldsymbol{x} \in \mathcal{I}^l) : \boldsymbol{x} \in \bigcup_{l=1}^{L} \mathcal{J}^l_R\right\},$$
$$\text{where : } \mathcal{J}^l_R = \begin{cases} \mathcal{I}^l & \text{if } \exists \boldsymbol{x}' \in \mathcal{I}^1 : h(\boldsymbol{x}') \ge 0 \\ \emptyset & \text{otherwise.} \end{cases}$$

Figure 4 shows an example of a one-dimensional function $g(\cdot)$ with an interval-based partition. Figure 4(a) plots a traditional piecewise constant approximation, using the average value of $g(\cdot)$ over each interval. In contrast, the conservative and relaxed models build downward and upward approximations (Figure 4 (b) and (c)), respectively, yielding a feasible solution and an optimality gap.

Remark 1. Models $[G_C]$ and $[G_R]$ yield a lower bound and an upper bound of $[G^*]$, respectively.

By construction, $[G^*]$ is infeasible if and only if $[G_R]$ is infeasible. Therefore, $[G_R]$ provides a certificate of feasibility. Let us now assume that $[G^*]$ is feasible. Under some regularity conditions on the function $g(\cdot)$, $[G_R]$ provides a certificate of optimality, as stated in Remark 2.

Remark 2. Assume that $g(\cdot)$ is k-Lipschitz continuous over $\mathcal{X}$. Define $\varepsilon > 0$. Let l_R be such that the set $\mathcal{I}^{l_R}$ contains an optimal solution of $[G_R]$. If the diameter of $\mathcal{I}^{l_R}$ is less than $\frac{\varepsilon}{k}$, then there exists a feasible solution in $\mathcal{I}^{l_R}$ within ε of the optimum of $[G^*]$.

To see this, let $\overline{\boldsymbol{x}}_R^g$ be a maximizer of $g(\cdot)$ over $\mathcal{I}^{l_R}$; and let $\overline{\boldsymbol{x}}_R^h \in \mathcal{I}^{l_R}$ such that $h(\overline{\boldsymbol{x}}_R^h) \geq 0$. By construction, $\overline{\boldsymbol{x}}_R^h$ is a feasible solution of $[G^*]$. From Lipschitz continuity and the assumption on the diameter of $\mathcal{I}^{l_R}$, we have $g(\overline{\boldsymbol{x}}_R^h) \geq g(\overline{\boldsymbol{x}}_R^g) - k\|\overline{\boldsymbol{x}}_R^g - \overline{\boldsymbol{x}}_R^h\| \geq g(\overline{\boldsymbol{x}}_R^g) - \varepsilon$. Because the optimum of the $[G_R]$ relaxation is achieved over $\mathcal{I}^{l_R}$, $g(\overline{\boldsymbol{x}}_R^g)$ is an upper bound of $[G^*]$, that is, for all $\forall \boldsymbol{x} \in \mathcal{X}$ such that $h(\boldsymbol{x}) \geq 0$, $g(\boldsymbol{x}) \leq g(\overline{\boldsymbol{x}}_R^g)$. Thus, $g(\overline{\boldsymbol{x}}_R^h) \geq Z[G^*] - \varepsilon$, where $Z[G^*]$ is the $[G^*]$ optimum.

Remark 2 underscores the role of the relaxed model $[G_R]$ in providing global optimality guarantees. In stark contrast, the conservative model $[G_C]$ and typical approximation schemes can lead to local optima—notably, when discretization is granular around a local optimum but coarse around the global optimum (Figure 4 (a) and (b)). Moreover, the result shows that the relaxed model can provide a certificate of optimality even when the discretization is only "locally" granular—around the $[G_R]$ solution—but not necessarily across the entire feasible region $\mathcal{X}$ (Figure 4(c)).

Translating these principles into an effective algorithm, however, raises two questions. The first one is how to minimize and maximize $g(\cdot)$ and $h(\cdot)$ in each set of the partition—in theory, this is as hard as the overall problem $[G^*]$. In our setting, this aspect is considerably simplified due to the monotonicity of the demand function (Lemma 2). The second one is how to reach granular discretization "locally" but not "globally" (to preserve tractability). We propose an adaptive procedure that iteratively refines the discretization based on the solutions of the conservative and relaxed models, and acceleration strategies using the local convexity of the demand function (Lemma 2).

5.2. Discretized Conservative and Relaxed Models

We proceed by interval-based discretization to build piecewise constant approximations of $f^{-1}(\cdot)$. Specifically, we define discretized values $(A_{od}^l)_{l \in \mathcal{L}_{od}}$ of the variable α_{od}, indexed in increasing order with $A_{od}^1 = 0$ and $A_{od}^{|\mathcal{L}_{od}|+1} = 1$. We define the following binary variables:

$$\beta_{od}^l = 1 \text{ if } \alpha_{od} = A_{od}^l \text{ for } o,d \in \mathcal{R},\ l \in \mathcal{L}_{od};\quad 0 \text{ otherwise.}$$

We introduce a conservative model $[M_C]$ and a relaxed model $[M_R]$, which both eliminate the nonconvexities of the function f^{-1} and can thus be solved as MISOCPs. In practical terms, these approximations involve underestimating and overestimating passenger demand for any level of service, respectively. In $[M_C]$, Equation (32) is replaced by Equations (33)–(36), so that $A_{od}^l \leq \alpha_{od} \leq A_{od}^{l+1}$ and $f^{-1}(A_{od}^{l+1}) \leq \tilde{\tau}_{od}$ for some $l \in \mathcal{L}_{od}$. In $[M_R]$, Equation (32) is replaced by Equations (37)–(40), so that $A_{od}^l \leq \alpha_{od} \leq A_{od}^{l+1}$ and $f^{-1}(A_{od}^l) \leq \tilde{\tau}_{od}$ for some $l \in \mathcal{L}_{od}$:

$$[M_C] \sum_{l \in \mathcal{L}_{od}} f^{-1}(A_{od}^{l+1})\,\beta_{od}^l \leq \tilde{\tau}_{od},\ \forall o,d \in \mathcal{R}, \tag{33}$$

$$\alpha_{od} \geq \sum_{l \in \mathcal{L}_{od}} A_{od}^l \beta_{od}^l,\ \forall o,d \in \mathcal{R}, \tag{34}$$

Figure 4. (Color online) Nonconvex Function $g(\cdot)$, with Piecewise Constant Approximations

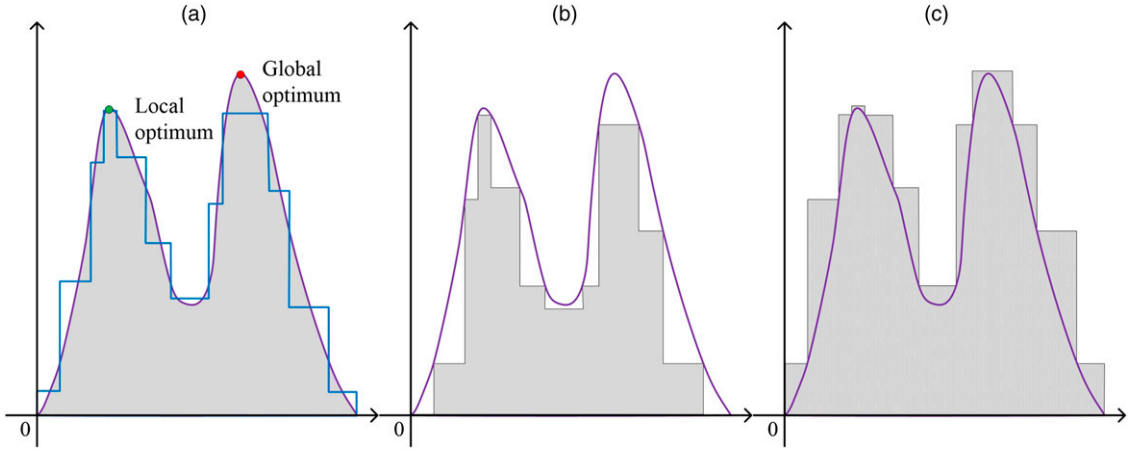

Notes. (a) Traditional approximation. (b) Conservative model. (c) Relaxed model.

Figure 5. (Color online) Example of S-Curve Function $f^{-1}(\cdot)$ and Feasible Regions of Models $[M^*]$, $[M_C]$, and $[M_R]$

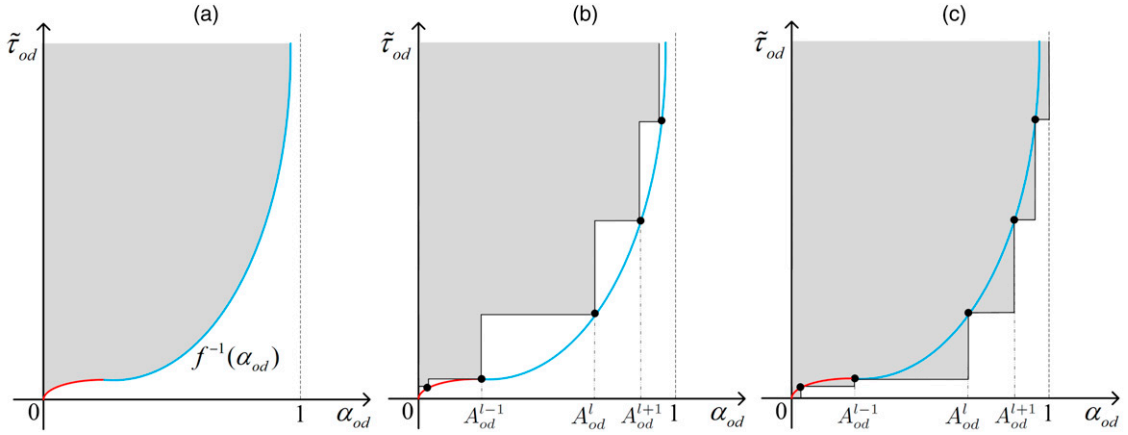

Notes. (a) M^* feasible region. (b) M_C feasible region. (c) M_R feasible region.

$$\alpha_{od} \le \sum_{l \in \mathcal{L}_{od}} A_{od}^{l+1} \beta_{od}^{l}, \quad \forall o,d \in \mathcal{R}, \tag{35}$$

$$\sum_{l \in \mathcal{L}_{od}} \beta_{od}^{l} = 1, \quad \forall o,d \in \mathcal{R}. \tag{36}$$

$$[M_R] \sum_{l \in \mathcal{L}_{od}} f^{-1}(A_{od}^{l}) \beta_{od}^{l} \le \tilde{\tau}_{od}, \quad \forall o,d \in \mathcal{R}, \tag{37}$$

$$\alpha_{od} \ge \sum_{l \in \mathcal{L}_{od}} A_{od}^{l} \beta_{od}^{l}, \quad \forall o,d \in \mathcal{R}, \tag{38}$$

$$\alpha_{od} \le \sum_{l \in \mathcal{L}_{od}} A_{od}^{l+1} \beta_{od}^{l}, \quad \forall o,d \in \mathcal{R}, \tag{39}$$

$$\sum_{l \in \mathcal{L}_{od}} \beta_{od}^{l} = 1, \quad \forall o,d \in \mathcal{R}. \tag{40}$$

Figure 5 illustrates the discretization schemes of $[M_C]$ and $[M_R]$. The feasible region of Model $[M_C]$ is contained in that of $[M^*]$; vice versa, the feasible region of $[M_R]$ contains that of $[M^*]$. Therefore, $[M_C]$ and $[M_R]$ provide lower and upper bounds of $[M^*]$, respectively, and both bounds become tighter as the discretization becomes more granular. This is stated in Proposition 2.

Proposition 2. *Let $Z[\cdot]$ denote the optimum of a model. Let $[M_C]$ and $[M'_C]$ (respectively, $[M_R]$ and $[M'_R]$) refer to the conservative (respectively, relaxed) model with two discretizations $\mathcal{L}_{od}$ and $\mathcal{L}'_{od}$ such that $\mathcal{L}'_{od} \subseteq \mathcal{L}_{od}$ for all $o,d \in \mathcal{R}$. It holds that $Z[M'_C] \le Z[M_C] \le Z[M^*] \le Z[M_R] \le Z[M'_R]$.*

5.3. Adaptive Discretization

We propose an adaptive discretization approach that dynamically updates the sets $\boldsymbol{A}_{od}$ to refine discretization around "promising" regions. The algorithm dynamically enlarges the feasible region of $[M_C]$ (Figure 6(a)) and reduces that of $[M_R]$ (Figure 6(b)). As such, it can be seen as a column generation approach for tackling nonconvex functions in otherwise-tractable optimization models.

Theorem 1 formalizes Remark 2 for our problem. It shows, again, that (i) the relaxed model $[M_R]$, unlike the conservative model $[M_C]$, provides optimality guarantees, and that (ii) the solution of the relaxed model can be certifiably near-optimal with only a "locally" granular discretization.

Theorem 1. *Define $\varepsilon > 0$. Let $(\boldsymbol{\alpha}^R, \tilde{\boldsymbol{\tau}}^R, \boldsymbol{u}^R)$ be an optimal solution of $[M_R]$. For each $o,d \in \mathcal{R}$, let $l(o,d)$ be such that $A_{od}^{l(o,d)} \le \alpha_{od}^R \le A_{od}^{l(o,d)+1}$. There exists $K>0$ such that, if $\alpha_{od}^R - A_{od}^{l(o,d)} \le K\varepsilon$ for all $o,d \in \mathcal{R}$, then $(f(\tilde{\boldsymbol{\tau}}^R), \tilde{\boldsymbol{\tau}}^R, \boldsymbol{u}^R)$ is a feasible solution of $[M^*]$ within ε of the global optimum.*

Theorem 1 highlights that optimality guarantees require granular discretization around the $[M_R]$ solution. In a traditional static discretization scheme, coarse discretization can thus lead to poor solutions or loose bounds (or both). Conversely, a granular discretization across the entire solution space can guarantee near-optimality but comes at great costs in terms of tractability. In contrast, we propose an adaptive discretization approach to build a granular discretization "locally" (to guarantee near-optimality) but to keep a coarse discretization elsewhere (to retain tractability).

Let $(\boldsymbol{\alpha}^R, \tilde{\boldsymbol{\tau}}^R, \boldsymbol{u}^R)$ denote the optimal solution of $[M_R]$ in a given iteration, with A_{od}^l such that $A_{od}^l \le \alpha_{od}^R \le A_{od}^{l+1}$. A simple adaptive discretization approach would be to add the midpoint $((A_{od}^l + A_{od}^{l+1})/2)$ for each O-D pair (o, d). This approach ensures worst-case convergence in $\mathcal{O}\left(\frac{1}{\varepsilon}\right)$ iterations.

Our adaptive discretization approach strengthens this simple approach in two ways:

1. We alternate between $[M_C]$ and $[M_R]$. Relying solely on the $[M_R]$ solution guarantees convergence (Theorem 1), but leveraging the $[M_C]$ solution orients the search toward "promising" solutions. As such, our adaptive discretization scheme can be viewed as

Figure 6. (Color online) Adaptive Discretization Scheme (Section 5.3) and Acceleration Based on Local Convexity (Section 5.4)

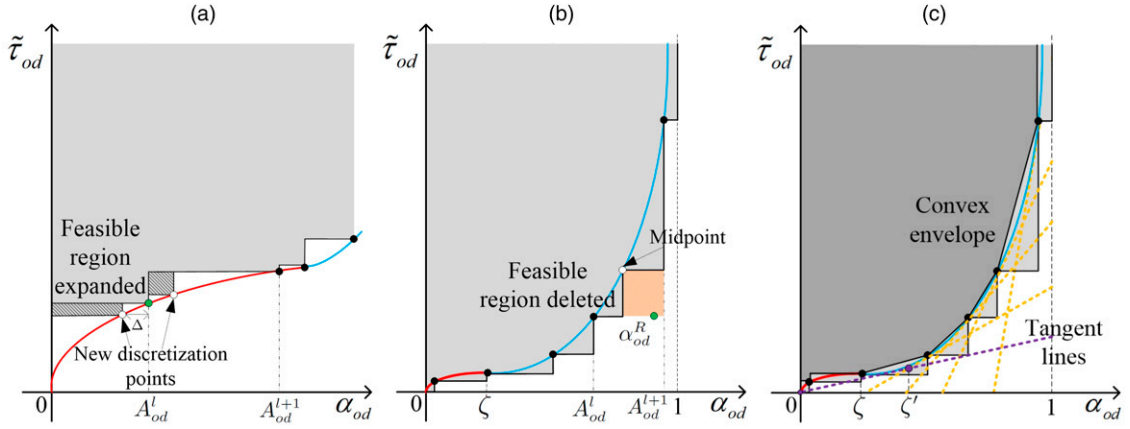

Notes. (a) Adaptive discretization in M_C. (b) Adaptive discretization in M_R. (c) Convexity-based acceleration.

alternating between exploitation—by creating "promising" variables from $[M_C]$—and exploration—by eliminating infeasible relaxations and avoiding local optima, from $[M_R]$. Moreover, at each iteration our approach updates a lower bound (from $[M_C]$) and an upper bound (from $[M_R]$).

2. Instead of systematically adding the midpoint $((A^l_{od}+A^{l+1}_{od})/2)$, we propose a more "local" adaptive discretization procedure, tailored to the latest $[M_C]$ solution. Specifically, if the $[M_C]$ solution lies in an existing point $(A^l_{od}, f^{-1}(A^l_{od}))$, we add the two points $A^l_{od}-\Delta$ and $A^l_{od}+\Delta$ into $\boldsymbol{A}_{od}$, where Δ is a small discretization unit (Figure 6(a)), as long as $\Delta \le ((A^l_{od}-A^{l-1}_{od})/2)$ and $\Delta \le ((A^{l+1}_{od}-A^l_{od})/2)$. This is consistent with our exploitation objective: since the $[M_C]$ solution is our most "promising" incumbent, we refine its neighborhood in subsequent iterations. This case where the $[M_C]$ solution lies in a point $(A^l_{od}, f^{-1}(A^l_{od}))$ is the most common one in our experiments, but not the only one. We present all adaptive discretization cases in Online Appendix EC.2.2.

In contrast, the $[M_R]$ solution is a poorer indicator of solution quality (because it is infeasible to $[M^*]$). Therefore, we leverage adaptive discretization to tighten the upper bound as much as possible. Therefore, we insert the midpoint $((A^l_{od}+\alpha^R_{od})/2)$ into $\boldsymbol{A}_{od}$, where $\boldsymbol{\alpha}^R$ is the $[M_R]$ solution and l is such that $A^l_{od} < \alpha^R_{od} \le A^{l+1}_{od}$. This makes the previous $[M_R]$ solution infeasible (Figure 6(b)).

5.4. Acceleration Based on Local Convexity

We further exploit the S-shaped structure of the demand function (Lemma 2) to accelerate adaptive discretization. Let $\zeta \in (0,1)$ be such that $f^{-1}(\cdot)$ is convex over $[\zeta,1]$ ($\zeta = 0.25$ for DRO and $\zeta = 0.5$ for MNL). We partition $\mathcal{L}_{od}$ into $\mathcal{L}^1_{od} = \{l \in \mathcal{L}_{od} \,|\, A^l_{od} < \zeta\}$ and $\mathcal{L}^2_{od} = \{l \in \mathcal{L}_{od} \,|\, A^l_{od} \ge \zeta\}$.

First, we define Model $[M^c_C]$ to build a convex envelope over $\mathcal{L}^2_{od}$, by relaxing the integrality constraints $\beta^l_{od} \in \{0,1\}$ for $l \in \mathcal{L}^2_{od}$ (Figure 6(c)). This tightens the lower bound of $[M^*]$ by constructing a piecewise linear (as opposed to piecewise constant) approximation over $[\zeta,1]$.

At the same time, $[M^c_C]$ has a larger solution space than $[M_C]$, and is more computationally intensive. We thus only relax the integrality of variables β^l_{od} adaptively for O-D pairs (o,d) with solutions α^C_{od} that fall in the relevant interval $[\zeta,1]$. We refer to this hybrid acceleration strategy (a middle ground between Models $[M_C]$ and $[M^c_C]$) as Model $[M^a_C]$.

Proposition 3. *It holds that* $Z[M_C] \le Z[M^a_C] \le Z[M^c_C] \le Z[M^*]$.

Similarly, we can tighten Model $[M_R]$ by adding tangent lines to $f^{-1}(\cdot)$. Unlike in convex optimization, however, we cannot add them whenever $\alpha_{od} \in [\zeta,1]$ (where the function $f^{-1}(\cdot)$ is locally convex) because it could eliminate feasible solutions over $[0,\zeta]$ (where it is not). Namely, we seek $\zeta' \ge \zeta$ such that, for all $\alpha^R_{od} \in [\zeta',1]$, the tangent lines at α^R_{od} tighten $[M_R]$ without eliminating feasible solutions (Figure 6(c)). We refer to the resulting relaxed model as $[M^t_R]$.

Tangent lines are valid cuts only if $f^{-1}(0)$ is finite (Proposition 4). This is the case for the DRO function (in which case $\zeta' = 0.5$) but not for MNL (in which case we simply apply $[M_R]$).

Proposition 4. *If* $f^{-1}(0)$ *is finite, let* ζ' *be the root of* $f^{-1}(0) - f^{-1}(\zeta') = -\zeta'(f^{-1})'(\zeta')$. *Then,* $\zeta' \in [\zeta,1]$ *and adding Constraints* (41) *to* $[M_R]$ *provides a tighter upper bound of* $[M^*]$:

$$\tilde{\tau}_{od} - f^{-1}(A^l_{od}) \ge \left(f^{-1}\right)'(A^l_{od})\left(\alpha_{od} - A^l_{od}\right),$$
$$\forall o,d \in \mathcal{R},\ \forall l \in \{l' \in \mathcal{L}_{od} \,|\, A^{l'}_{od} \ge \zeta'\}. \tag{41}$$

Online Appendix EC.2.2 details our adaptive discretization approach with our convexity-based acceleration.

5.5. Summary and Solution Algorithm

We have developed three conservative models: $[M_C]$, $[M_C^c]$, and $[M_C^a]$; and two relaxed models: $[M_R]$ and $[M_R^t]$. Our adaptive discretization scheme (Algorithm 1 in Online Appendix EC.2.3) iteratively solves $[M_C^a]$ and $[M_R^t]$, which both rely on piecewise constant or piecewise linear approximations of the nonlinear function (using the same discretized values), and provide lower and upper bounds of $[M^*]$, respectively. Therefore, the algorithm updates an optimality gap at each iteration. It terminates when the optimality gap reaches a prespecified threshold, and Theorem 1 guarantees finite convergence. Ultimately, this adaptive discretization algorithm provides an exact solution approach to a broad class of mixed-integer nonconvex optimization problems comprising a "tractable part" (an MISOCP, in our case) but also a nonconvex part (the demand constraint, in our case).

6. Computational Results

We test our algorithm with taxi data from the NYC Taxi & Limousine Commission (2019). To capture other transportation modes, we scale demand by a factor $S \geq 1$. We use data from Uber Elevate (2016) to define characteristics of UAM systems. We detail the experimental setup in Online Appendix EC.3. We solve each model with CPLEX 12.5 (Intel Xeon CPU (3.0 GHz), 128 GB RAM).

In this real-world environment, the model comprises 4.2 million variables, including 1.3 million binary ones, and 18.5 million constraints, including 1,000 conic ones and 1,300 nonconvex ones. Combined with its nonconvex structure, the sheer size of the model makes it very hard to solve.

We refer to a static run of Model A as $Sta(A)$, and to an adaptive approach iterating between Models A and B as $Ada(A, B)$. Using this nomenclature, our generic adaptive discretization algorithm is $Ada(M_C, M_R)$, and our full algorithm (Algorithm 1) is $Ada(M_C^a, M_R^t)$.

6.1. Convergence of the Adaptive Discretization Algorithm

Figure 7 plots the lower bound (LB) and the upper bound (UB) of the generic algorithm $Ada(M_C, M_R)$ and the full—accelerated—one $Ada(M_C^a, M_R^t)$. Both algorithms reach a 1% optimality gap in less than 30 iterations (i.e., 15 $[M_R]$ runs, 15 $[M_C]$ runs). Our adaptive discretization approach thus yields a globally optimal solution of the nonconvex optimization model $[M^*]$. Moreover, the accelerated algorithm converges in fewer iterations, showing the benefits of leveraging local convexity by selectively enlarging the feasible region (Model $[M_C^a]$) and tightening the relaxation (Model $[M_R^t]$). We provide more comparisons in Section 6.3.

Online Appendix EC.3.2 shows that the algorithm converges in comparable numbers of iterations with the DRO and MNL demand functions. The MNL model leads to larger models and longer runtimes, because it estimates a nonzero traffic share on more O-D pairs, and because the formulation cannot be tightened as with the DRO formulation (Online Appendix EC.1.2). Nonetheless, the performance of adaptive discretization is robust to the demand model specification.

6.2. Value of Dynamic Discretization

Table 2 evaluates our adaptive discretization approach against static benchmarks, with discretization units of 0.1, 0.05, and 0.01. These benchmarks span coarse to granular discretization, with 15,168, 26,544, and 127,644 total discretization points, respectively, across all O-D pairs. The starting point of Algorithm 1 corresponds to a discretization unit of 0.1.

The main observation is that Algorithm 1 consistently outperforms static methods by a wide margin. Computational times increase with demand, because $[M_C^a]$ and $[M_R^t]$ become more time-consuming as more vertiports get constructed. Yet, our algorithm is robust to the demand scale, converging to a 1% gap in 13 to 25 iterations and within 1,000 minutes across all instances. Interestingly, our adaptive discretization algorithm adds few new discretized points (up to 1,131), thus creating a granular discretization around the optimal solution while keeping it coarse elsewhere.

Under coarse static discretizations (units of 0.1 and 0.05), the static benchmark $Sta(M_C^a)$ is fast but yields much worse solutions—with a profit reduction of 25%–50% with $S = 2$ and of 2%–20% under higher demand. Overall, whenever $Sta(M_C^c)$ terminates faster than Algorithm 1, it generates lower profits by at least 3.72%. Under granular discretization (unit of 0.01), $Sta(M_C^c)$ becomes much more computationally intensive, and even ends up losing its computational benefits compared with our adaptive approach. Moreover, static discretization still returns consistently inferior solutions than Algorithm 1 (by 1%–3%), even when allowed to run longer. Finally, the upper bound from $Sta(M_R^t)$ is also at least 2% worse than the one from Algorithm 1, even under granular discretization.

In summary, our adaptive discretization algorithm dominates static discretization benchmarks in all aspects: better solutions, shorter computational times, and stronger solution guarantees.

6.3. Benefits of Algorithm Design

Finally, Table 3 shows the benefits of our algorithm design compared with simpler adaptive discretization schemes. Note, first, the benefits of leveraging local convexity by alternating between Models $[M_C^a]$ and $[M_R^t]$, as opposed to the simpler models $[M_C]$ and $[M_R]$. Indeed, $Ada(M_C, M_R)$ requires two to four more

Figure 7. (Color online) Convergence of the Adaptive Discretization Algorithms: $Ada(M_C, M_R)$ and $Ada(M_C^a, M_R^t)$

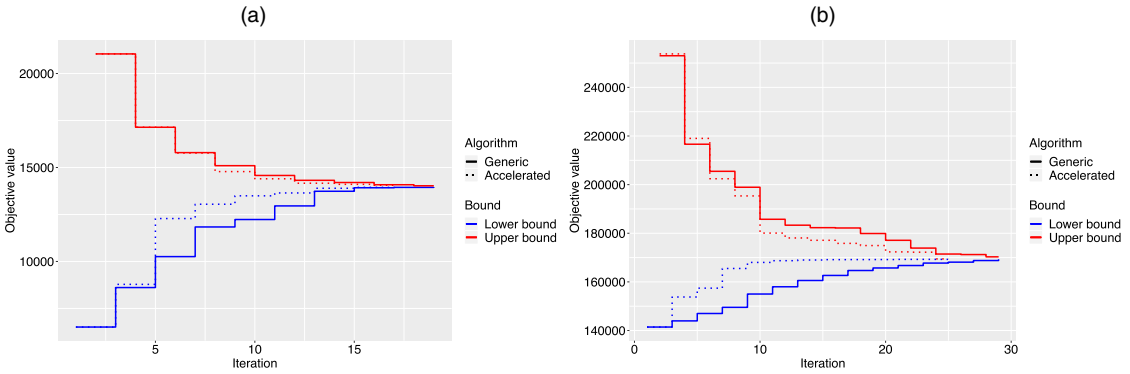

Notes. (a) Lower and upper bounds with $S = 2$. (b) Lower and upper bounds with $S = 8$.

iterations and longer computational times—by 12%–188%. Moreover, $Ada(M_C^c, M_R^t)$, which relaxes binary variables whenever possible, requires same or fewer iterations, but much longer runtimes—by 85%–374%. These results underscore the value of tightening the conservative and relaxed models based on local convexity but doing so parsimoniously.

Second, our algorithm benefits from alternatively solving the conservative and relaxed models. In comparison, $Ada(M_C^c, \emptyset)$, which solves $[M_C^c]$ until the solution stops improving, yields a solution that is 3%–14% inferior. This confirms that adaptive discretization based on feasible solutions alone can lead to local optima, underscoring the value of the model's relaxation to guide the primal search in the adaptive discretization scheme (Theorem 1). The last benchmark, $Ada(\emptyset, M_R^t)$, only solves $[M_R^t]$. As per Theorem 1, it would converge to optimality; to ensure an apples-to-apples comparison, we let it run for as long as Algorithm 1. Upon termination, all upper bounds are worse than those of Algorithm 1: just as the discretization generated by $[M_R^t]$ is instrumental in guiding $[M_C^a]$ toward

Table 2. Comparison of Our Algorithm and Static Discretization as a Function of the Demand Scaling Factor

Unit	Method	Metric	$S = 2$	$S = 3$	$S = 4$	$S = 5$	$S = 6$	$S = 7$	$S = 8$
Algorithm 1		Lower bound (LB)	13,971.99	35,065.73	56,405.69	81,018.29	118,283.72	148,939.61	169,272.80
$Ada(M_C^a, M_R^t)$		Upper bound (UB)	14,052.53	35,212.78	56,497.93	81,634.77	119,146.72	149,477.64	169,450.92
		Optimality gap	< 1%	< 1%	< 1%	< 1%	< 1%	< 1%	< 1%
		# iterations	17	13	19	19	15	13	25
		Time (minutes)	0.80	0.90	3.14	5.43	125.95	142.66	960.19
		# $[M_C^a]$ points	164	139	237	299	326	287	616
		# $[M_R^t]$ points	104	79	201	211	206	209	515
		% O-D shares in $[\zeta, 1]$	23.1%	23.1%	31.3%	37.5%	46.4%	44.8%	44.8%
0.10	$Sta(M_C^c)$	Objective	6,790.41	27,898.12	47,851.71	74,009.50	111,927.74	140,359.46	152,600.34
		Gap from LB	51.40%	20.44%	15.17%	8.65%	5.37%	5.76%	9.85%
		Time (minutes)	0.11	0.17	0.39	1.39	1.77	2.59	63.78
	$Sta(M_R^t)$	Objective	21,042.74	42,561.47	76,114.02	108,831.35	141,986.96	195,672.23	252,048.38
		Gap from UB	49.74%	20.87%	34.72%	33.31%	19.17%	30.90%	48.74%
		Time (minutes)	0.03	0.04	0.09	0.17	0.29	0.38	1.91
0.05	$Sta(M_C^c)$	Objective	10,400.97	28,590.66	51,295.45	75,944.54	113,888.58	142,367.76	165,269.69
		Gap from LB	25.56%	18.47%	9.06%	**6.26%**	3.72%	4.41%	**2.36%**
		Time (minutes)	0.15	0.33	1.59	**7.05**	12.46	29.53	**>1440**
	$Sta(M_R^t)$	Objective	20,325.32	42,108.25	73,751.40	106,053.24	134,679.99	167,226.51	230,128.41
		Gap from UB	44.64%	19.58%	30.54%	29.91%	13.04%	11.87%	35.81%
		Time (minutes)	0.03	0.05	0.10	0.18	0.30	0.40	2.42
0.01	$Sta(M_C^c)$	Objective	13,290.34	34,039.23	55,213.70	80,019.26	116,629.03	144,898.41	166,131.25
		Gap from LB	4.88%	**2.93%**	**2.11%**	**1.23%**	**1.40%**	**2.71%**	**1.86%**
		Time (minutes)	0.38	**0.98**	**20.46**	**45.23**	**184.03**	**>1440**	**>1440**
	$Sta(M_R^t)$	Objective	15,221.18	36,773.70	59,195.68	93,454.56	121,561.07	154,778.59	181,197.32
		Gap from UB	8.32%	4.43%	4.77%	14.48%	2.03%	3.55%	6.93%
		Time (minutes)	0.04	0.07	0.38	0.49	0.53	1.42	5.43

Notes. # $[M_C^a]$/$[M_R^t]$ points, number of discrete points added (to 15,168 at start) in the adaptive discretization procedure; >1,440, static model is not solved to optimality within 24 hours. Bold font indicates instances with longer computational times than those for our adaptive discretization algorithm.

Table 3. Benefits of Algorithm Design as a Function of the Demand Scaling Factor

Method	Metric	$S = 2$	$S = 3$	$S = 4$	$S = 5$	$S = 6$	$S = 7$	$S = 8$
Algorithm 1	Solution (LB)	13,971.99	35,065.73	56,405.69	81,018.29	118,283.72	148,939.61	169,272.80
$Ada(M_C^a, M_R^t)$	Upper bound (UB)	14,052.53	35,212.78	56,497.93	81,634.77	119,146.72	149,477.64	169,450.92
	# iterations	17	13	19	19	15	13	25
	Time (minutes)	0.80	0.90	3.14	5.43	125.95	142.66	960.19
$Ada(M_C, M_R)$	Optimality gap	< 1%	< 1%	< 1%	< 1%	< 1%	< 1%	< 1%
	# iterations	19	15	21	21	19	15	29
	Time (minutes)	0.98	1.16	8.68	15.64	141.04	163.53	1,379.18
$Ada(M_C^c, M_R^t)$	Optimality gap	< 1%	< 1%	< 1%	< 1%	< 1%	< 1%	< 1%
	# iterations	17	13	19	19	15	11	23
	Time (minutes)	3.79	4.26	9.41	10.43	233.61	368.12	1815.88
$Ada(M_C^c, \emptyset)$	Lower bound	13,330.15	30,316.85	54,268.91	77,413.79	114,542.66	144,017.84	161,614.84
	Gap from LB	4.59%	13.54%	3.79%	4.45%	3.16%	3.30%	4.52%
$Ada(\emptyset, M_R^t)$	Upper bound	14,210.93	35,765.33	56,915.31	82,809.32	119,400.23	151,039.75	176,759.28
	Gap from UB	1.13%	1.57%	0.74%	1.44%	0.21%	1.05%	4.31%

stronger solutions, the one generated by $[M_C^a]$ also guides $[M_R^t]$ toward stronger bounds.

Therefore, a key driver of our algorithm's performance is the alternation between the conservative model $[M_C^a]$ and the relaxed model $[M_R^t]$. Again, this approach provides a Pareto improvement over all benchmarks in terms of solution quality, computational times, and solution guarantees.

7. Managerial Insights Toward UAM Vertiport Networks

We address our three practical questions regarding the structure of UAM networks, the benefits of vertiport optimization, and the drivers of UAM profitability. We first conduct a case study using the NYC taxi data, which captures granular transportation patterns. We use a demand scaling factor of $S = 2$, approximately capturing current demand from taxis and ride-sharing. In other cities, we estimate commuting patterns using the LEHD Origin-Destination Employment Statistics (LODES) data from the U.S. Census Bureau (2020). We aggregate the data at the zip code level and define travel demand for morning commutes (patterns would be reversed in the evening).

Recall that, in our model, μ_{od} denotes the average travel time reduction—relative to ground transportation—needed to attract customers. We calibrate it uniformly across O-D pairs, and denote it by $\overline{\mu}$. One extreme, $\overline{\mu} = 1$, reflects a high price or a strong aversion toward UAM; whereas at the other extreme, $\overline{\mu} = 0$, UAM captures the entire market as long as UAM is faster than ground transport (reflecting a competitive price or strong enthusiasm for UAM). In between, $\overline{\mu}$ captures the price point and customer expectations. We set a default value of $\overline{\mu} = 40\%$ (Uber Elevate 2016).

7.1. Structure of UAM Networks

7.1.1. NYC Taxi Data. Figure 8 shows that UAM is most competitive on long-distance O-D pairs. With $\overline{\mu} = 0.4$, the UAM network serves O-D pairs with high demand and long travel times. As $\overline{\mu}$ decreases, UAM also serves O-D pairs with lower demand, but still with long travel times. This is because the en route portion needs to be long enough to offset the "fixed costs" of UAM trips due to ground travel to and from the vertiports and to passenger pooling. In our case study, UAM is used between Manhattan and the city's airports, but ground transportation still dominates within Manhattan travel (due to shorter travel times) and interborough travel (due to lower demand).

Constructed vertiport locations are reported in Table 4. Although UAM networks are not yet deployed in practice, a close analogy is Uber Copter, which maintained two heliports—in Manhattan and at JFK Airport. Similarly, for $\overline{\mu} = 0.40$, our UAM network relies on three vertiports—JFK, Clinton East (Manhattan), and Astoria (near LaGuardia Airport). Interestingly, passenger trips are longer to/from the selected vertiport in Astoria than to/from an alternative vertiport in LaGuardia itself; however, by being closer to Manhattan, the Astoria vertiport leads to shorter flights (hence, higher service reliability and less battery consumption) and shorter detours for unserved passengers. These patterns underscore the complex operating trade-offs underlying vertiport network design.

As $\overline{\mu}$ decreases, the UAM network grows in a nested fashion. Indeed, almost all vertiports constructed with a given value of $\overline{\mu}$ also get constructed with lower values of $\overline{\mu}$. The only exception is that decreasing $\overline{\mu}$ from 0.35 to 0.34 replaces the vertiport in Lincoln Square East by the almost-identical one in Upper West Side South. Although our model is static, this result suggests opportunities to deploy a phased approach to UAM network expansion, by starting with a few "obvious" vertiports, and then adding more vertiports as UAM penetration increases.

7.1.2. U.S. Census Data. Figure 9 shows the UAM networks for four metropolitan areas, with a budget of 10

Figure 8. (Color online) UAM Traffic Shares for All O-D Pairs as a Function of Demand (Log Scale), Ground Transportation Times (Log Scale), and $\overline{\mu}$

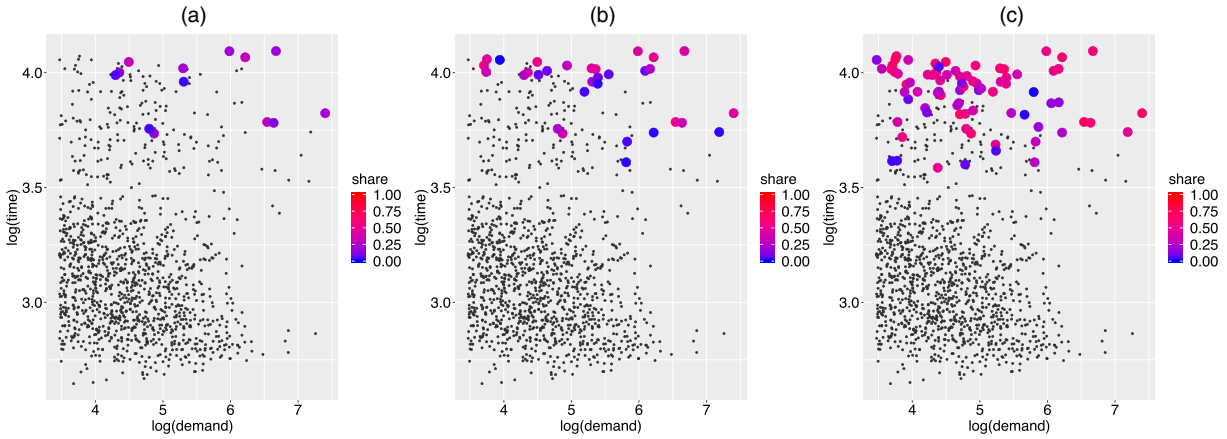

Notes. Small black dots indicate O-D pairs that are not served by UAM; the UAM traffic shares α_{od} on the other O-D pairs are indicated larger dots. (a) $\overline{\mu} = 0.40$. (b) $\overline{\mu} = 0.37$. (c) $\overline{\mu} = 0.33$.

vertiports in each city (see Online Appendix EC.4.2 for the others). These results confirm that UAM primarily serves long-distance trips (e.g., between downtown areas and suburbs), although some networks allow for a few shorter trips (e.g., northwest of Boston). Hence, UAM can serve as a more natural alternative to self-driving or commuter rail rather than taxi or ride-sharing. The structure of UAM networks varies from one city to another. For instance, Los Angeles has a star network, with disjoint origins (in residential areas) and concentrated destinations (in downtown). In contrast, San Francisco has an interconnected network where several regions serve departing and arriving passengers. Others (e.g., Dallas, Boston) fall between. There is thus no one-size-fits-all recipe for UAM deployment; instead, cities need to plan UAM systems based on geographic, urban and commuting dynamics (as shown here), as well as other considerations (e.g., transit, equity).

7.1.3. Concentrated Networks. One of our questions involved characterizing the structure of UAM networks between a "dispersion strategy" (many scattered vertiports) and a "concentration strategy" (a few central vertiports). In traditional network planning, this question balances capital and operating expenses: all else equal, larger networks (e.g., more fulfillment centers in logistics, generators in power systems, relief areas in humanitarian operations) are more expensive to build but lead

Table 4. Constructed Vertiports for Different Customer Aspiration Levels, Represented by the Demand Parameter $\overline{\mu}$

Demand parameter $\overline{\mu}$	0.40	0.39	0.38	0.37	0.36	0.35	0.34	0.33
JFK Airport (Springfield Gardens)	✓	✓	✓	✓	✓	✓	✓	✓
Midtown Center (Grace Building)	×	×	×	×	×	✓	✓	✓
Clinton East (Hell's Kitchen)	✓	✓	✓	✓	✓	✓	✓	✓
Clinton West (Pier 88)	×	×	×	✓	✓	✓	✓	✓
TriBeCa (Pier 26)	×	×	×	×	×	×	✓	✓
Lincoln Square East (Lincoln Center)	×	×	×	×	×	✓	×	×
Upper West South (Carousel Parking)	×	×	×	×	×	×	✓	✓
Garment District (Bus Terminal)	×	×	×	×	×	✓	✓	✓
Gramercy (Peter's Field)	×	×	×	×	×	×	✓	✓
Newark Airport (Newark Helistop)	×	×	×	×	×	×	×	✓
Astoria (Rainey Park)	✓	✓	✓	✓	✓	✓	✓	✓
LaGuardia Airport (Terminals C&D)	×	×	×	×	×	×	×	×
Other 20 candidate vertiport locations	×	×	×	×	×	×	×	×
# of vertiports constructed	3	3	3	4	4	7	9	10
# O-D pairs with service	13	16	20	31	33	39	67	78
Traffic share (average)	16.8%	20.1%	21.2%	25.2%	29.8%	31.7%	34.0%	39.0%
Traffic share (25th percentile)	11.9%	8.3%	3.3%	6.5%	9.2%	10.2%	17.3%	24.2%
Traffic share (75th percentile)	21.1%	28.8%	35.3%	42.0%	48.0%	49.0%	51.7%	57.3%

Note. ✓(respectively, ×) denotes that the candidate vertiport is (respectively, is not) constructed.

Figure 9. (Color online) UAM Networks

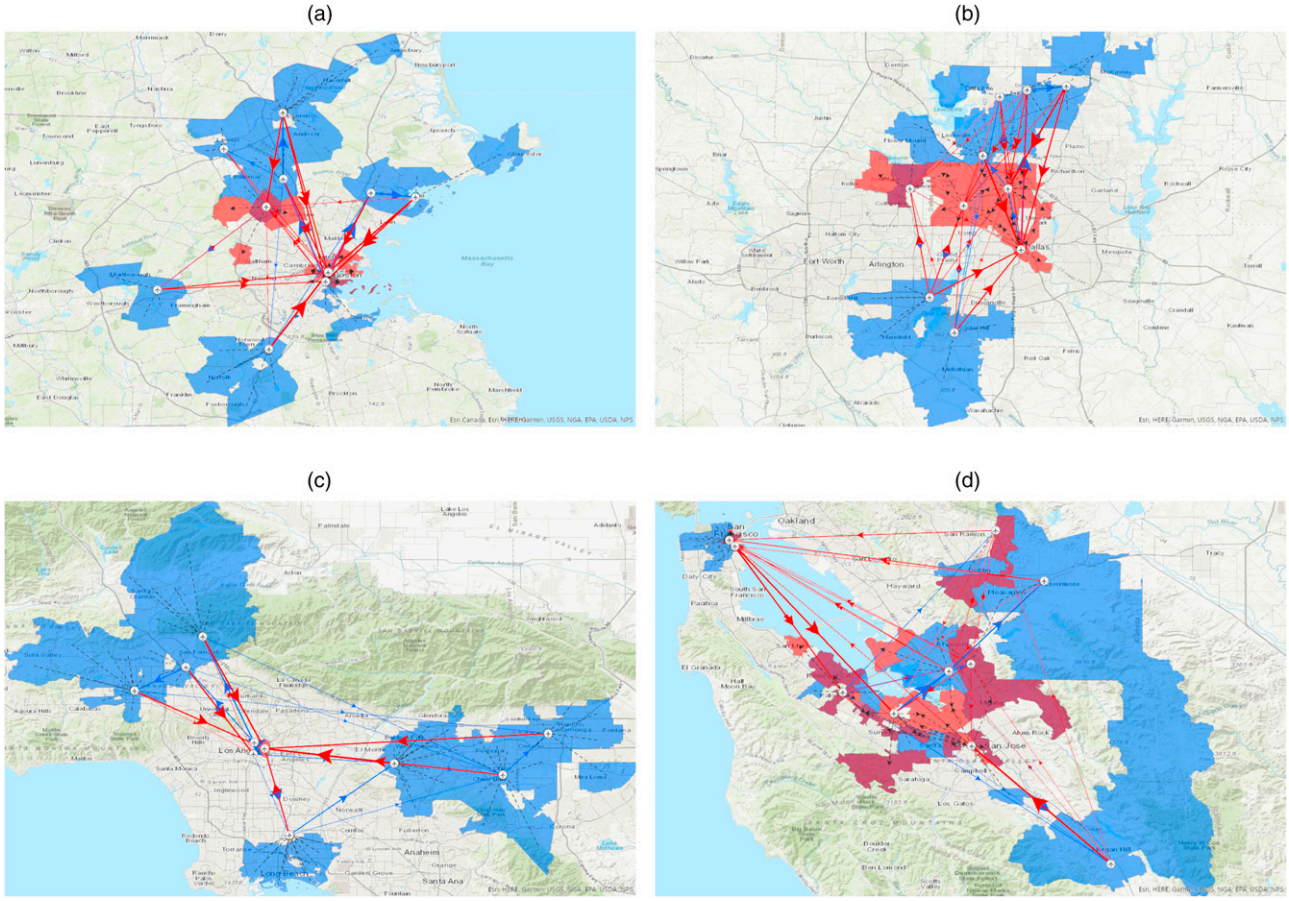

Notes. Each map shows vertiports (icons), passenger-carrying trips (solid lines mostly pointed to the vertiports in urban areas) and repositioning trips (solid lines of rebalancing between vertiports), catchment areas (i.e., the zip codes with origins, destinations and both, as indicated by the arrows of the passenger-carrying trips), and passengers' assignments to departure and arrival vertiports (dashed lines). (a) Boston. (b) Dallas. (c) Los Angeles. (d) San Francisco.

to cheaper operations (e.g., lower costs in distribution, unit commitment, disaster management). To study this question, we constrain the model to build—and use—a given number of vertiports. In these experiments, we scale demand down so the optimal network has around six to eight vertiports.

Table 5 reports the relative changes from a five-vertiport baseline. It shows that the operating profit (which does not account for vertiport costs) is consistently maximized with an intermediate network size. As expected, in some instances (e.g., Dallas from eight to nine vertiports), a larger network enables larger-scale operations: larger fleet, higher vehicle utilization, higher revenues and higher operating costs. However, spatial-temporal patterns are such that more repositioning flights are needed to maintain high reliability levels across the network—so operating costs increase more than revenues. More surprisingly, in other instances (e.g., San Francisco from eight to nine vertiports, shown in Figure 10), a larger network leads to smaller-scale operations: smaller fleet, lower vehicle utilization, lower revenues and lower operating costs. With eight vertiports, the network features global synergies by consolidating operations. Notably, Vertiport 6 serves as an arrival vertiport from Vertiports 1 and 2, enabling large repositioning flows toward Vertiport 3. With nine vertiports, the new vertiport (Vertiport 10) provides a more convenient option for nearby passengers but it thus reduces consolidation around Vertiport 9, leading to smaller repositioning flows in the northern region. As a result, the new vertiport breaks the synergies within the network, leading to two disconnected sub-networks (shown in Figure 10(b)).

Ultimately, we find that operating profitability is *not* monotonically increasing with the network size. In San Francisco for instance, operating profits decrease, increase, and decrease again when the network grows from six to nine vertiports. Thus, network expansions can break existing synergies across vertiports, and further expansions can restore such synergies. This result establishes a stark contrast with canonical network planning. On the one hand, more vertiports cover more

Table 5. Impact of UAM Network Size on Operating Profitability

City	Metric	Five vertiports	Six vertiports	Seven vertiports	Eight vertiports	Nine vertiports
BOS	Revenue	100%	**106.4%**	102.3%	99.7%	98.3%
	Fleet cost	100%	116.7%	122.2%	**88.9%**	116.7%
	Fleet utilization rate	**100%**	72.6%	79.6%	87.4%	71.7%
	Operating profit	100%	**108.4%**	101.2%	98.2%	97.6%
	Net profit	100%	**101.6%**	91.7%	87.4%	85.4%
DAL	Revenue	100%	114.4%	137.8%	138.4%	**142.1%**
	Fleet cost	**100%**	136.4%	181.8%	172.7%	181.8%
	Fleet utilization rate	**100%**	84.8%	87.3%	80.9%	83.5%
	Operating profit	100%	112.8%	124.9%	**134.5%**	132.2%
	Net profit	100%	103.3%	105.8%	**116.9%**	112.4%
LA	Revenue	100%	114.6%	126.3%	**132.6%**	132.3%
	Fleet cost	**100%**	120.8%	141.7%	162.5%	162.5%
	Fleet utilization rate	**100%**	95.4%	88.6%	81.5%	81.1%
	Operating profit	100%	113.9%	124.7%	**129.9%**	129.3%
	Net profit	100%	111.2%	**118.4%**	118.4%	116.9%
SF	Revenue	100%	139.1%	122.1%	**139.6%**	128.8%
	Fleet cost	**100%**	141.7%	133.3%	141.7%	133.3%
	Fleet utilization rate	100%	108.5%	95.5%	**109.3%**	104.6%
	Operating profit	100%	143.4%	130.7%	**147.8%**	136.9%
	Net profit	100%	145.9%	124.9%	**147.8%**	129.5%

Notes. "Operating profit" excludes vertiport construction costs. Net profit, full profit expression (Equation (26)).

demand hotspots, reducing passengers' ground travel times. But more vertiports also reduce passenger consolidation (hence, increasing pooling times at departure vertiports) and vehicle consolidation (hence, decreasing service reliability). Back to our question, we often find benefits of a "concentration strategy," as opposed to a "dispersion strategy" to induce consolidation and synergies in UAM networks. This finding echoes recent research on alleviating the "wild goose chase" in ride-sharing through temporal and spatial pooling (e.g., batching, taxi stands; Hu 2020).

7.1.4. Operational Dynamics. Whereas this paper primarily deals with strategic UAM network planning, our results also shed light on interesting operating dynamics in UAM networks:

- All vertiports are not created equally: some vertiports primarily serve departures and others primarily serve arrivals. In fact, some vertiports serve as satellite vertiports for recharging purposes and do not cater to passengers at all (e.g., one downtown vertiport in Figure 9(c)).
- Spatial coupling: Although UAM mainly serves high-demand and long-distance markets, the pattern is not monotonic (Figure 8). That is, some "attractive" markets will not receive a service, whereas less attractive ones will be served due to synergistic markets in their vicinity.
- Cost of repositioning: The incidence of repositioning trips can even exceed 50% (see Online Appendix EC.4.1 for an example), indicating the costs of spatial imbalances on UAM operations.

Figure 10. (Color online) Increasing the Network Size for San Francisco

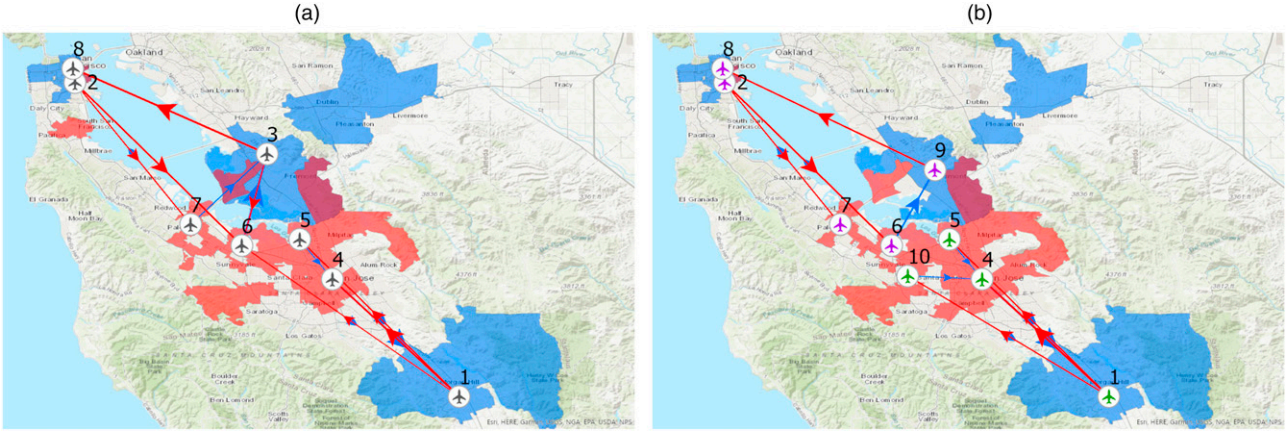

Notes. (a) Eight vertiports. (b) Nine vertiports.

• Cost of reliability: Ensuring a high level of service is key to attract customers but also comes at high operating costs due to larger fleets and extensive repositioning (see Online Appendix EC.4.1).

These dynamics highlight the complex interplay between vehicle routing, vertiport capacities, battery charging and passenger pooling. Strategic planning in UAM systems therefore involves not only anticipating future travel patterns, but also identifying the role of each vertiport in UAM networks and subsequent UAM operations. We further expand on that point in the next section.

7.2. Benefits of UAM Optimization with Demand and Operating Endogeneity

We compare our integrated approach to four benchmarks (see Online Appendix EC.4.3 for details).

• *p-median*: select "central" vertiports based on passengers' origins and destinations (akin to the clustering approach from Lim and Hwang (2019) and Willey and Salmon (2021))

• *exogenous demand*: replace the endogenous demand function with exogenous traffic share estimates, by (i) assigning the average traffic share in our optimized network to all O-D pairs ("avg"); and (ii) assigning to each O-D pair its own optimized correct traffic share ("opt")

• *exogenous operations*: ignore battery charging, and fix reliability levels and pooling times; and optimize vertiport network and flight and repositioning flows (without our queuing network)

• *exogenous demand and operations*: combine the two above benchmarks

For each benchmark, we derive the vertiport network, fix the corresponding variables, and re-evaluate the profits using Model [M^*]. As such, any benchmark solution is a feasible solution to [M^*]; so the [M^*] solution will be at least as strong as each benchmark solution. However, we are interested in the magnitude of the profit differences between the benchmarks and the optimized solution, as well as the relative performance of the benchmarks. Results are reported in Table 6.

The *p*-median solution leads to 22%–53% reduction in profitability compared with our optimized one. This underscores that demographic information is blind to downstream UAM operations and to the drivers of passenger demand. For instance, the *p*-median approach treats all O-D pairs equally, ignoring that UAM is more competitive on long-distance O-D pairs. This result highlights complex intricacies surrounding UAM network planning versus canonical coverage-maximizing location settings. Moreover, it suggests that demographic-based benchmarks—although natural—can perform poorly in practice, thus motivating dedicated vertiport planning strategies.

Similarly, treating demand as exogenous leads to significant profit deterioration. With a uniform traffic share on all O-D pairs (obtained from, say, population-based surveys), the model fails to capture variations in passenger demand across the network, leading to a 10%–30% profit reduction. In contrast, this benchmark performs much better with differentiated traffic share estimates (e.g., from more advanced and granular surveys). In other words, all O-D pairs are not created equally when it comes to UAM demand; instead, significant benefits can be derived by adjusting market penetration at a more granular level, as opposed to relying on one-size-fits-all estimates. Yet, even with ex post optimal traffic shares, treating demand as exogenous induces a 2%-4% profit reduction. This stresses the need to properly appraise passenger demand variations as a function of level of service, as against merely estimating demand for each O-D pair.

Along the same lines, ignoring operating endogeneity leads to large losses. In fact, the approach with exogenous operations and endogenous demand performs the worst, by far. This may appear surprising, because this approach integrates the demand function, as opposed to relying on exogenous traffic share estimates. However, by ignoring operating dynamics, it wrongly estimates UAM trip times, leading to poor demand estimates. Finally, even with the best possible demand estimates, ignoring operating endogeneity yields 3%–10% profit reductions compared with our integrated approach.

Collectively, these observations underline the benefits of capturing the interdependencies between strategic UAM network planning, tactical UAM operations, and passenger demand. From a practical standpoint, future UAM operations therefore need to be supported by

Table 6. Benefits of Integrated Optimization Approach Compared with Optimization Benchmarks

	Boston		Dallas		Los Angeles		San Francisco	
Optimization Approaches	Profit	Change	Profit	Change	Profit	Change	Profit	Change
Integrated	816,742	—	1,949,232	—	950,441	—	2,374,492	—
p-median	553,879	−32.2%	1,435,838	−26.3%	447,046	−53.0%	1,836,683	−22.6%
Exogenous demand (avg.)	706,006	−13.6%	1,647,196	−15.5%	657,185	−30.9%	2,124,948	−10.5%
Exogenous demand (opt.)	798,735	−2.2%	1,872,195	−4.0%	920,888	−3.1%	2,317,748	−2.4%
Exogenous operations	284,868	−65.1%	894,175	−54.1%	218,066	−77.1%	1,786,115	−24.8%
Exogenous demand (avg.) and operations	691,776	−15.3%	1,598,848	−18.0%	588,142	−38.1%	2,022,273	−14.8%
Exogenous demand (opt.) and operations	786,949	−3.6%	1,784,155	−8.5%	857,679	−9.8%	2,235,697	−5.8%

Table 7. Impact of Technical eVTOL Characteristics and Demand Parameters on UAM Profitability

		Boston		Dallas		Los Angeles		San Francisco	
	Setup	Profit	Change	Profit	Change	Profit	Change	Profit	Change
	Baseline	816,742	—	1,949,232	—	950,441	—	2,374,492	—
Technical parameters	Increase $\frac{b^{dpt}}{b^{chg}}$ by 25%	749,158	−8.3%	1,681,874	−13.7%	836,191	−12.0%	1,992,455	−16.1%
	Increase $\frac{b^{dpt}}{b^{chg}}$ by 50%	678,223	−17.0%	1,499,277	−23.1%	739,190	−22.2%	1,743,429	−26.6%
	Increase c^E by 25%	804,506	−1.5%	1,877,839	−3.7%	937,660	−1.3%	2,237,006	−5.8%
	Increase c^E by 50%	765,039	−6.3%	1,771,575	−9.1%	877,200	−7.7%	2,184,146	−8.0%
	Increase $\boldsymbol{c}^F$ by 25%	802,641	−1.7%	1,837,231	−5.7%	928,315	−2.3%	2,246,986	−5.4%
	Increase $\boldsymbol{c}^F$ by 50%	797,011	−2.4%	1,791,513	−8.1%	912,242	−4.0%	2,195,853	−7.5%
Demand parameter	Increase $\overline{\mu}$ by 10%	639,414	−21.7%	1,461,578	−25.0%	640,006	−32.7%	1,914,985	−19.4%
	Increase $\overline{\mu}$ by 20%	392,512	−51.9%	939,268	−51.8%	348,686	−63.3%	1,520,576	−36.0%
	Increase $\overline{\mu}$ by 30%	146,840	−82.0%	445,479	−77.1%	98,265	−89.7%	957,590	−59.7%
	Increase $\overline{\mu}$ by 40%	47,969	−94.1%	160,297	−91.8%	0.0	−100%	267,354	−88.7%
	Increase $\overline{\mu}$ by 50%	0	−100%	34,576	−98.2%	0	−100%	21,713	−99.1%

tailored analytics capabilities, especially when it pertains to strategic network planning.

7.3. Drivers of UAM Profitability

We conclude by reporting UAM profitability in Table 7 with various eVTOL acquisition costs c^E, eVTOL operating costs $\boldsymbol{c}^F$, depletion-charging ratios b^{dpt}/b^{chg}, and demand parameters $\overline{\mu}$.

As expected, UAM profitability depends on the technical characteristics of eVTOL aircraft. However, some of these variations remain moderate. For instance, even massive increases in eVTOL acquisition and operating costs (by up to 50%) induce moderate profit decreases (within 10%). In comparison, a 25% deterioration in the depletion-charging ratio reduces profits by more than 10% in three of four cities. This underscores the role of battery performance as a driver of vehicle utilization in UAM networks, especially given the focus on long-distance flights. However, overall, the impact of technical specifications remains much smaller than that of the demand parameter $\overline{\mu}$. Indeed, even a 20% increase in $\overline{\mu}$ (from 0.4 to 0.48) leads to a 36%–63% profit reduction—driven by the need to ensure a high level of service on O-D pairs to capture even moderate traffic shares. A 40%–50% increase in $\overline{\mu}$ could even make the UAM operations unprofitable altogether.

From a practical standpoint, these findings suggest that, to become successful, UAM operators require not only supply-side advances in eVTOL technologies but also demand-side efforts to manage customer expectations and generate passenger demand. Such initiatives can take the form of pricing strategies to attract a customer base, public relations campaigns to alleviate safety and environmental concerns, and marketing campaigns to promote a new mode of transportation.

8. Conclusion

This paper proposes an original model to optimize the number, locations and capacities of vertiports toward UAM. The model captures interdependencies between strategic UAM planning, tactical UAM operations, and customer demand. It includes a "tractable part" (mixed-integer second-order conic optimization) and a nonconvex demand function.

To tackle it, we designed an algorithm that builds piecewise constant approximations of the model's nonconvexities, iterating between a *conservative model* (which provides a feasible solution) and a *relaxed model* (which provides a solution guarantee). We proposed an adaptive discretization procedure to iteratively enlarge the feasible region of the conservative model (to focus on "promising" regions) and reduce that of the relaxed model (to eliminate local optima). This adaptive discretization scheme converges to a global optimum, thanks to the relaxed model. The algorithm provides an exact solution approach to a broad class of mixed-integer nonconvex programs. In our experiments, it returns solutions within a 1% optimality gap in 15–30 iterations, and it strongly dominates all benchmarks in terms of solution quality, runtimes, and solution guarantees.

From a practical standpoint, we found that optimized UAM networks vary widely across metropolitan areas as a function of geographic, urban, and commuting patterns. Nonetheless, a few commonalities emerge. One is that UAM networks rely on a few centralized vertiports as opposed to many scattered ones, highlighting the benefits of consolidation in UAM operations to facilitate vehicle routing and passenger pooling. Another commonality is that UAM is most competitive on long-distance markets, therefore providing a more natural alternative to commuter rail and self-driving rather than taxi and ride-sharing. We also found that UAM profitability is highly sensitive to network planning optimization and to customer expectations, perhaps even more so than to vehicle and battery specifications. Therefore, the success of UAM operations not only requires more research and development in eVTOL technologies but also needs tailored analytics-based capabilities to optimize strategic planning and market-based efforts to drive customer demand.

This research can be extended in two major directions. From a practical standpoint, we focused on network planning—a prominent strategic challenge currently faced by future UAM operators. This research, however, can be extended with dedicated optimization models to support downstream UAM operations (e.g., vehicle routing optimization, the design of on-demand versus scheduled services, disruption management, service pricing) and a dedicated simulation environment to estimate the impact of various vertiport planning architectures. From a methodological standpoint, the high-quality solutions obtained with our adaptive discretization algorithm open up new questions on the performance of this approach for other mixed-integer nonconvex optimization problems.

References

A3 by Airbus (2018) Vahana: The next technological breakthrough in urban air mobility. Accessed April 1, 2022, www.airbus-sv.com/projects/1.

Adelman D (2007) Price-directed control of a closed logistics queueing network. *Oper. Res.* 55(6):1022–1038.

AVweb (2019) Boeing autonomous eVTOL makes first flight. Accessed April 1, 2022, www.avweb.com/recent-updates/business-military/boeing-autonomous-evtol-makes-first-flight/.

Baur S, Hader M (2020) The high-flying industry: Urban Air Mobility takes off. Technical report, Roland Berger, Munich, Germany.

Binder R, Garrow L, German B, Mokhtarian P, Daskilewicz M, Douthat T (2018) If you fly it, will commuters come? Predicting demand for eVTOL urban air trips. *Proc. AIAA Conf.* (American Institute of Aeronautics and Astronautics, Reston, VA), 1–41.

Boland N, Hewitt M, Marshall L, Savelsbergh M (2017) The continuous-time service network design problem. *Oper. Res.* 65(5): 1303–1321.

Booz Allen Hamilton (2018) Urban air mobility (UAM) market study. Technical report, NASA, Washington, D.C.

Boyaci B, Zografos KG, Geroliminis N (2015) An optimization framework for the development of efficient one-way car-sharing systems. *Eur. J. Oper. Res.* 240(3):718–733.

Brown A, Harris W (2018) A vehicle design and optimization model for on-demand aviation. *Proc. AIAA/ASCE/AHS/ASC Structures, Structural Dynamics, and Materials Conf.* (American Institute of Aeronautics and Astronautics, Reston, VA), 1–46.

El Ghaoui L, Oks M, Oustry F (2003) Worst-case value-at-risk and robust portfolio optimization: A conic programming approach. *Oper. Res.* 51(4):543–556.

Garrow LA, German BJ, Leonard CE (2021) Urban air mobility: A comprehensive review and comparative analysis with autonomous and electric ground transportation for informing future research. *Transporation Res., Part C Emerging Techn.* 132:103377.

Garrow LA, German B, Mokhtarian P, Glodek J (2019) A survey to model demand for eVTOL urban air trips and competition with autonomous ground vehicles. *Proc. AIAA Aviation 2019 Forum* (American Institute of Aeronautics and Astronautics, Reston, VA), 1–45.

Ha TH, Lee K, Hwang JT (2019) Large-scale design-economics optimization of eVTOL concepts for urban air mobility. *Proc. AIAA Scitech Forum* (American Institute of Aeronautics and Astronautics, Reston, VA), 1–18.

He L, Mak HY, Rong Y, Shen ZJM (2017) Service region design for urban electric vehicle sharing systems. *Manufacturing Service Oper. Management* 19(2):309–327.

Hu M (2020) Spatial or temporal pooling solves wild goose chase. Preprint, submitted October 5, https://dx.doi.org/10.2139/ssrn.3676065.

Jaillet P, Song G, Yu G (1996) Airline network design and hub location problems. *Location Sci.* 4(3):195–212.

Joby Aviation (2021) Our story. Accessed April 1, 2022, www.jobyaviation.com.

Johnston T, Riedel R, Sahdev S (2020) To take off, flying vehicles first need places to land. Technical report, McKinsey & Company, New York.

Kabra A, Belavina E, Girotra K (2020) Bike-share systems: Accessibility and availability. *Management Sci.* 66(9):3803–3824.

Kleinbekman IC, Mitici MA, Wei P (2018) eVTOL arrival sequencing and scheduling for on-demand urban air mobility. *Proc. IEEE/AIAA 37th Digital Avionics Systems Conf.* (IEEE, New York), 1–7.

Lagos F, Boland N, Savelsbergh M (2020) The continuous-time inventory-routing problem. *Transportation Sci.* 54(2):375–399.

Lederer PJ, Nambimadom RS (1998) Airline network design. *Oper. Res.* 46(6):785–804.

Lim E, Hwang H (2019) The selection of vertiport location for on-demand mobility and its application to seoul metro area. *Internat. J. Aeronautical Space Sci.* 20(1):260–272.

NYC Taxi & Limousine Commission (2019) TLC trip record data. Accessed April 1, 2022, www1.nyc.gov/site/tlc/about/tlc-trip-record-data.page.

Pavone M (2015) Autonomous mobility-on-demand systems for future urban mobility. *Autonomes Fahren* (Springer, Berlin), 399–416.

Pradeep P, Wei P (2018) Energy efficient arrival with RTA constraint for urban eVTOL operations. *Proc. AIAA Aerospace Sci. Meeting* (American Institute of Aeronautics and Astronautics, Reston, VA), 1–13.

Uber Elevate (2016) Fast-forwarding to a future of on-demand urban air transportation. Accessed April 1, 2022, www.uber.com/elevate.pdf.

U.S. Census Bureau (2020) Longitudinal employer-household dynamics (LEHD). Accessed April 1, 2022, lehd.ces.census.gov/data/.

Vascik PD, Hansman RJ (2017) Evaluation of key operational constraints affecting on-demand mobility for aviation in the Los Angeles basin. *Proc. 17th AIAA Aviation Tech., Integration, and Oper.* (American Institute of Aeronautics and Astronautics, Reston, VA), 1–20.

Vascik PD, Hansman RJ (2019) Development of vertiport capacity envelopes and analysis of their sensitivity to topological and operational factors. *Proc. AIAA Scitech Forum* (American Institute of Aeronautics and Astronautics, Reston, VA), 1–26.

Vertical Flight Society (2021) eVTOL aircraft directory. Technical report, Vertical Flight Society, Fairfax, VA.

Vu DM, Hewitt M, Boland N, Savelsbergh M (2020) Dynamic discretization discovery for solving the time-dependent traveling salesman problem with time windows. *Transportation Sci.* 54(3): 703–720.

Whitt W (1984) Open and closed models for networks of queues. *ATT Bell Laboratory Tech. J.* 63(9):1911–1979.

Willey LC, Salmon JL (2021) A method for urban air mobility network design using hub location and subgraph isomorphism. *Transportation Res., Part C Emerging Tech.* 125:102997.